Organic & Biomolecular Chemistry

Accepted Manuscript

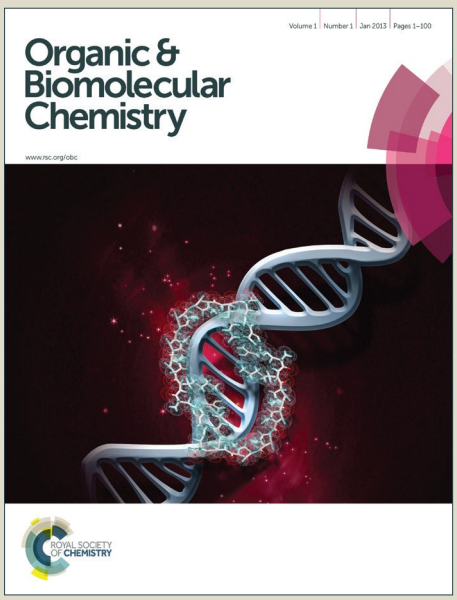

ROYAL SOCIETY OF CHEMISTRY

www.rsc.org/obc

Organic &Biomolecular Chemistry RSCPublishing

PAPER

Rational design, synthesis and molecular modeling studies of novel anti-oncological alkaloids against melanoma

Cite this: DOI: 10.1039/x0xx00000x

Received ooth January 2012,
Accepted ooth January 2012

DOI: 10.1039/x0xx00000x

www.rsc.org/

Adel S. Girgis,*[a] Siva S. Panda,[b] Aladdin M. Srour,[c] Hanaa Farag,[a] Nasser S. M. Ismail,[d] Mohamed Elgendy,[e] Amal K. Abdel-Aziz[f] and Alan R. Katritzky‡[,b]

3D-Pharmacophore and 2D-QSAR modeling studies describe the anti-oncological properties of spiro-alkaloids. The dispiro[2*H*-indene-2,3'-pyrrolidine-2',3''-[3*H*]indole]-1,2''(1''*H*, 3*H*)-diones **20-38** were prepared *via* 1,3-dipolar cycloaddition reactions of azomethine ylides (generated *in situ vi*a decarboxylative condensation of isatins **7-9** with sarcosine **10**) and 2-(arylmethylidene)-2,3-dihydro-1*H*-inden-1-ones **11-19** in refluxing ethanol. Some of the spiro-alkaloids (**21**, **22**, **29** and **37**) revealed potent antitumor properties against melanoma carcinoma cell lines (GaLa, LuPiCi and LuCa) utilizing the *in-vitro* SRB standard method exhibiting potency close to that of the standard reference doxorubicin.

Introduction

Basal cell carcinoma, squamous cell carcinoma and melanoma are three major types of skin cancer.[1] Malignant melanoma is a tumor that arises from melanocytic cells and primarily involves the skin.[2] Solar ultraviolet radiation, fair skin, dysplastic nevi syndrome and a family history of melanoma are major risk factors. Melanomas metastasize either by the lymphatic or by the hematogenous route.[3] Malignant melanoma is one of the most lethal cancers due to its high cellular proliferation rate and the early occurrence of metastases. Around 160,000 new cases of melanoma are diagnosed in the world each year, and procedures for effective treatment of melanoma are still not available. Increased surveillance with early diagnosis and accurate staging of the disease are important to increased survival.[4] Early stage melanoma (stage I/II) primary tumors can be cured surgically with more than 95% success rate.[5] On the other hand, late-stage (stage IV) metastatic melanoma is one of the most deadly forms of cancer, with a median survival of 7-9 months for patients with distant metastases.[6]

Vemurafenib (PLX4032, Zelboraf) (**1**) was approved in 2011 by the U.S. food and drug administration for treatment of late-stage melanoma.[7] Vemurafenib can be considered a bio-isosteric form of an indolyl derivative. Interest in the 2-oxindole scaffold is attributed to its kinase inhibitory properties.[8-12] Biological and/or pharmacological properties of many alkaloids and natural products containing the spiropyrrolidine-oxindole nucleus also encouraged the present study. For example, mitraphylline (**2**), isolated from *Uncaria tomentosa*, possesses potent antitumor properties against human brain cancer cell lines, neuroblastoma SKN-BE(2) and malignant glioma GAMG[13] while, spirotryprostatins A (**3**) and B (**4**) (isolated from the fermentation broth of *Aspergillus fumigatus*) are powerful inhibitors of the G2/M progression cell division in mammalian tsFT210 cells.[14,15] MI-888 (**5**) is currently in preclinical evaluation for the treatment of human cancer. MI-888 is a potent inhibitor of p53-MDM2 interaction capable of achieving rapid, complete and durable tumor regression in two types of xenograft models of human cancer with oral administration.[16] P53 protein is a nuclear transcription factor that functions as a tumor suppressor. It regulates the cell cycle by repairing DNA and inhibits growth of tumors.[17] MI-219 (**6**) is also a spiro-oxindole analogue binds to MDM2 with low nanomolar affinity, efficaciously blocks the MDM2-p53 protein-protein interaction in cells, reactivates p53 in cancer cells, and is still in pre-clinical stage (Figure 1).[18-21]

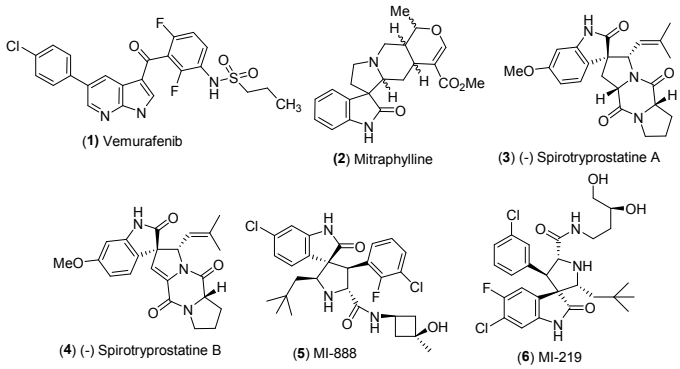

Figure 1 Pharmacological active indole-containing compounds.

The present study describes synthesis of novel dispiro[2*H*-indene-2,3'-pyrrolidine-2',3"-[3*H*]indoles] where the indolyl *N*-1" is linked to [(cyclic-amino)methylene] function. A possible role of the [(cyclic-amino)methylene] function is to provide a positive ionizable residue that may fit our candidate analogue in the pharmacophoric active site. The synthesized alkaloids within the present study will be screened against diverse human melanoma cell lines. 3D-pharmacophoric and 2D-QSAR (quantitative structure-activity relationship) studies are considered in the present work utilizing Discovery Studio 2.5 and Comprehensive Descriptors for Structural and Statistical Analysis (CODESSA-Pro) software. This allows a better understanding of the observed pharmacological activity and determines the most important structural parameters controlling bio-activity. These studies are also used to validate the observed bio-data.

Results and discussion

Chemistry

The targeted dispiro[2*H*-indene-2,3'-pyrrolidine-2',3"-[3*H*]indole]-1,2"(1"*H*, 3*H*)-diones **20-36** were prepared *via* 1,3-dipolar cycloaddition reactions of azomethine ylides, (generated *in situ via* decarboxylative condensation of isatin derivatives **7-9** with sarcosine **10** based on Grigg's methodology[22]) and 2-(arylmethylidene)-2,3-dihydro-1*H*-inden-1-ones **11-19** in refluxing ethanol. The reaction commences with nucleophilic attack of the amino group of sarcosine **10** on the 3-carbonyl function of indole derivative **7-9**, followed by dehydration to form a spiro-oxazalidinone system. This, expels carbon dioxide to generate a reactive, non-stabilized azomethine ylide, that undergoes *in situ* 1,3-dipolar cycloaddition with the exocyclic olefinic linkage of indenones **11-19** affording eventually spiro-alkaloids **20-36** (Scheme 1). The structures of the isolated products **20-36** were established *via* spectroscopic (IR, ^{1}H-NMR, ^{13}C-NMR, HRMS) and elemental analysis data.

For example, a representative of the synthesized dispiro-analogue family compound **20** exhibited a broad strong stretching vibration band at ν = 1707 cm^{-1} assigned to the overlapped carbonyls of ketonic and amidic functions. The ^{1}H-NMR spectrum of **20** revealed the pyrrolidinyl methylene protons H_2C-5', as a diastereotopic two spin system, that appeared as two triplets at δ_H = 3.57 and 4.07 due to mutual coupling, and coupling with the vicinal pyrrolidinyl methine proton *HC*-4'. The indanyl methylene protons H_2C-3 appear as diastereotropic protons giving two doublets at δ_H = 2.69 and 3.11, respectively. The methylene protons attached to the indolyl *N*-1" also appeared as diastereotopic protons (the upfield one appears as a doublet signal at δ_H = 4.16 however, the downfield one is overlapped with the pyrrolidinyl methine proton *HC*-4' forming a multiplet signal at δ_H = 4.36-4.45). The ^{13}C-NMR spectrum of **20** exhibited the pyrrolidinyl H*C*-4', H_2C-5' carbons at δ_C = 49.8 and 59.1, respectively and the piperidinyl carbons showed resonances at δ_C = 24.1 (H_2C-4), 25.9 (H_2C-3/5) and 52.0 (NH_2C-2/6), respectively. The spiro-carbons *C*-2 (*C*-3'), *C*-2' (*C*-3") were revealed at δ_C = 66.9 and 78.8, respectively. The indanyl H_2C-3 was located at δ_C = 35.4, while the oxindolyl *C*-2" and indanyl *C*-2 carbonyl carbons resonated at δ_C = 177.3 and 206.4, respectively. The ^{13}C-NMR spectra of other analogues possessing a (4-morpholinyl)methylene residue attached to the *N*-1" position, as exemplified by **21**, exhibited morpholinyl carbon resonances at δ_C = 51.0 (NCH_2) and 66.8 (OCH_2). For compound **29**, the piperazinyl carbon signals appeared at δ_C = 50.6 (NH_2C-2/6) and 54.9 (NH_2C-3/5) and the piperazinyl NCH_3 carbon at δ_C = 46.1.

In contrast to the reactions described above, a condensation involving isatin **9** (X = NCH_3), sarcosine **10** and 2-(arylmethylidene)-2,3-dihydro-1*H*-inden-1-ones **14** (R = 2,4-$Cl_2C_6H_3$) and **18** [R = 4-$(H_3C)_2NC_6H_4$] under the same reaction conditions afforded compounds **37**, **38**, instead of the expected dispiroindole of type **20-36** (Scheme 1). Mechanistic aspects of the reactions leading to **37**, **38** are unclear but the structures of these compounds were established by IR, ^{1}H-NMR, ^{13}C-NMR which revealed a pattern similar to that observed for compounds **20-36**. Stereochemical structure of compounds **20-38** were exhibited based on our previous single crystal X-ray studies of similar synthesized analogues under the same applied reaction conditions.[23,24]

Antitumor properties

Antitumor properties of the synthesized spiro-alkaloids **20-38** were screened against diverse melanoma human tumor cell lines (GaLa, LuPiCi and LuCa) utilizing the *in-vitro* Sulfo-Rhodamine-B (SRB) standard method.[23-31] From the results obtained (Table 1), it is apparent that most of the synthesized analogues exhibit mild antitumor properties against the melanoma cell lines tested. However, some of the compounds (**21, 22, 29** and **37**) reveal potent antitumor properties close to that of doxorubicin, the standard reference.

From the observed antitumor activity data, it is noticed that insertion of a bromine substituent at the 4'-position of the phenyl group in **22** (IC_{50} "concentration required to produce 50% inhibition of cell growth compared to control experimental" = 9.15, 2.92 and 1.15 μM against GaLa, LuPiCi and LuCa cell lines, respectively) greatly enhances the observed pharmacological properties relative to other electron-withdrawing (chlorine) or electron-donating (methyl, methoxy, dimethylamino) groups. On the other hand, insertion of a 4-(methylpiperazinyl) function as a cyclic-amino substituent attached through a methylene linker to the indolyl *N*-1" affords a promising antitumor active agent compared to the other adopted groups (piperidinyl and morpholinyl) as exhibited in compounds **27-29** (IC_{50} = 42.60, 52.08, 5.50; 29.56, 33.60, 3.62 and 13.62, 22.20, 2.62 μM against GaLa, LuPiCi and LuCa cell lines, respectively).

In order to better understand the observed antitumor properties and determine the most important structural parameters controlling bio-activity, computational chemistry studies were undertaken. Additionally, validation of the observed antitumor properties may be established *via* these studies.

Computational chemistry

3D-Pharmacophore modeling

The IUPAC definition of pharmacophore is "an ensemble of steric and electronic features that is necessary to ensure the optimal supramolecular interactions with a specific biological target and to trigger (or block) its biological response".[32] Pharmacophores are used in modern computational chemistry to define the essential features of one or more molecules with the same biological

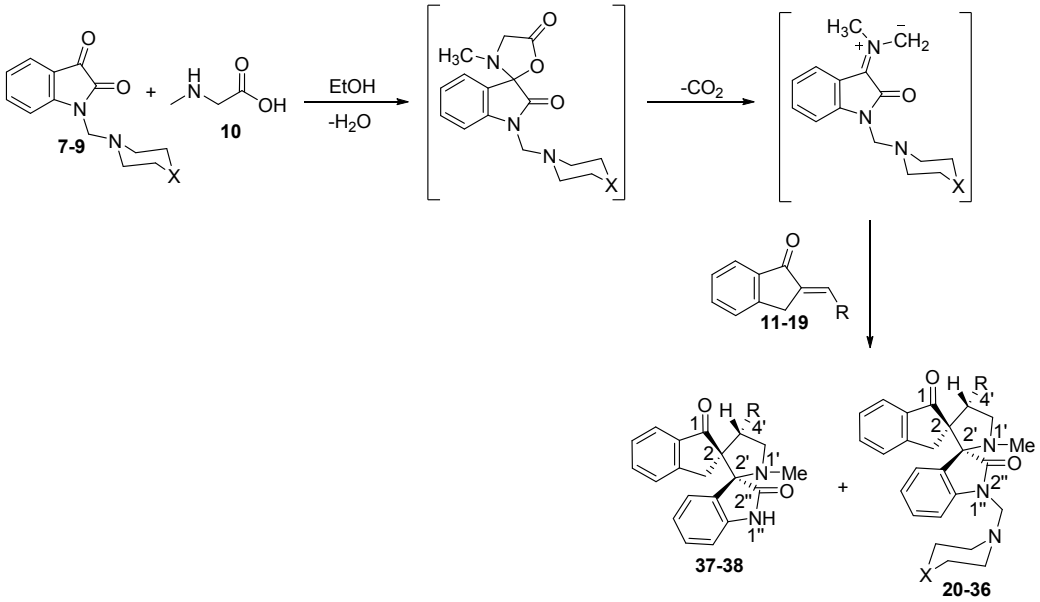

7, X = CH_2
8, X = O
9, X = NCH_3

11, R = Ph
12, R = 4-BrC_6H_4
13, R = 4-ClC_6H_4
14, R = 2,4-$Cl_2C_6H_3$
15, R = 4-$H_3CC_6H_4$
16, R = 4-$H_3COC_6H_4$
17, R = 3,4,5-$(H_3CO)_3C_6H_2$
18, R = 4-$(H_3C)_2NC_6H_4$
19, R = 2-Thienyl

37, R = 2,4-$Cl_2C_6H_3$
38, R = 4-$(H_3C)_2NC_6H_4$

20; R = Ph, X = CH_2
21; R = Ph, X = O
22; R = 4-BrC_6H_4, X = CH_2
23; R = 4-ClC_6H_4, X = CH_2
24; R = 4-ClC_6H_4, X = O
25; R = 2,4-$Cl_2C_6H_3$, X = CH_2
26; R = 2,4-$Cl_2C_6H_3$, X = O
27; R = 4-$H_3CC_6H_4$, X = CH_2
28; R = 4-$H_3CC_6H_4$, X = O
29; R = 4-$H_3CC_6H_4$, X = NCH_3
30; R = 4-$H_3COC_6H_4$, X = CH_2
31; R = 4-$H_3COC_6H_4$, X = O
32; R = 3,4,5-$(H_3CO)_3C_6H_2$, X = CH_2
33; R = 3,4,5-$(H_3CO)_3C_6H_2$, X = O
34; R = 4-$(H_3C)_2NC_6H_4$, X = CH_2
35; R = 4-$(H_3C)_2NC_6H_4$, X = O
36; R = 2-Thienyl, X = CH_2

Scheme 1 Synthetic routes towards dispiro[2*H*-indene-2,3'-pyrrolidine-2',3"-[3*H*]indoles] **20-38**.

activity. The 3D-pharmacophore study was performed using Discovery Studio 2.5 software (Accelrys Inc., San Diego, CA, USA) which permits 3D-pharmacophore generation, structural alignment, activity prediction and 3D-database creation.[33-35] 3D-pharmacophore protocol was used to generate predictive pharmacophores *via* aligning different conformations in which the molecules are likely to bind with the receptor. A given hypothesis may be combined with known activity data to create a 3D-pharmacophore model that identifies overall aspects of molecular structure governing bio-activity. 3D-pharmacophore was constructed using collections of molecules with activities ranging over a number of orders of magnitude. Pharmacophores explain the variability of bioactivity with respect to the geometric localization of the chemical features present in the molecules. The observed HYPOGEN identifies a 3D-array of four chemical features in case of GaLa and five features in case of LuPiCi and LuCa carcinoma cell lines which are common to the bio-active set compounds **20-36** that provides relative alignment for each input molecule, consistent with its binding mode to a proposed common receptor site.

The four chemical features of the GaLa pharmacophore are two hydrogen bonding acceptors (HBA-1, HBA-2) and two positive ionizables (PosIon-1, PosIon-2) (Figure 2, exhibits constraint distances and angles between features of the generated

GaLa 3D-pharmacophore). On the other hand, the LuPiCi and LuCa pharmacophores contain five chemical features, two hydrogen bonding acceptors (HBA-1, HBA-2), two hydrophobics (H-1, H-2) and a positive ionizable (PosIon) (Figures 3, 4). Table 2 exhibits fit values and estimated/predicted activities of the synthesized spiro-alkaloids **20-36** due to the generated 3D-pharmacophore models. Fit values are used for scoring the interaction taking place between a ligand and a pharmacophore. The quality of the mapping is indicated by the fit value. The computed fit value depends on two parameters: the weights assigned to the pharmacophore features and how close the features in the molecule are to the centres of the corresponding location constraints in the pharmacophore. Fit value is computed as follows: Fit = sum over mapped features f of weight (f)*[1-SSE(f)], where, SSE(f) = sum over location constraints c on f of $[D(c)/T(c)]^2$, where D = the displacement of the feature from the center of the location constraint, and T = the radius of the location constraint sphere for the feature (tolerance).

Through the pharmacophore mapping studies due to GaLa, LuPiCi and LuCa carcinoma cell lines (Figures S1-S3 of supporting information) it is apparent that the major structural factors affecting the potency of the synthesized compounds are related to their basic skeleton. Additionally, most of the estimated activities as well as the fit values derived from the generated pharmacophores are correlated to the experimentally observed bio-properties.

GaLa pharmacophore mapping studies exhibit that the indolyl and indanyl carbonyls are aligned with HBA-1, HBA-2, respectively while, the cyclicamino *N*-1 and pyrrolidinyl nitrogen (*N*-1') are aligned with PosIon-1, PosIon-2, respectively for the synthesized compounds **20-28, 30-36**. Compound **29** which is considered the most potent analogue among all the synthesized spiro-alkaloids against GaLa cell line (IC_{50} = 5.50, 4.75 μM corresponding to the observed and estimated potencies, respectively, fit value = 7.82) exhibits a slight deviation relative to the other synthesized derivatives where, the PosIon-1 is aligned with the piperazinyl *N*-4 (Figure S1 of supporting information). This alignment may explains the high potency of this analogue with a minimum error value (error between observed and estimated potencies = 0.75). This observation is also consistent with the mentioned SAR rules governing bio-properties, emphasizing the role of the piperazinyl function in enhancing the overall observed bio-properties among the other adopted cyclicamino residues (piperidinyl, morpholinyyl). Fitness variations of the synthesized compounds in the hypothesized GaLa pharmacophore due to their chemical structures determine their estimated potencies. For example compounds **21** and **22** that seem high potent analogues against GaLa cell line exhibit estimated IC_{50} values 23.43, 23.45 μM, respectively (fit value = 7.12). Although the error differences due to the observed and estimated values of these compounds are relatively high (error = -15.42, -14.30 for compounds **21** and **22**, respectively), their potencies are still preserved among all the other synthesized analogues. The mild potent agents against GaLa cell line **20, 23, 26** and **34** (observed IC_{50} = 28.12-38.16 μM) reveal estimated IC_{50} values = 25.52-33.22 μM (fit value = 6.97-7.09), which are also consistent with their bio-potencies among the other synthesized spiro-alkaloids. Compound **35**, which is considered experimentally inactive agent against GaLa cell line "reveals very low activity" (observed IC_{50} = 334.00 μM) shows also very low estimated anti-tumor behavior according to the hypothesized GaLa pharmacophore (estimated IC_{50} = 104.05 μM, fit value = 6.48).

LuPiCi pharmacophore mapping studies exhibit that the indolyl and indanyl carbonyls are aligned with HBA-1, HBA-2, respectively, the benzonide residues of the indolyl and indanyl functions are aligned with H-1 and H-2, respectively and the cylclicamino *N*-1 is aligned with PosIon for all the synthesized compounds **20-36** (Figure S2 of supporting information). The most potent agents against LuPiCi carcinoma cell line, compounds **21, 22** and **29** reveal estimated potencies conserving their bio-properties among all the synthesized analogues (IC_{50}= 3.20, 2.92, 3.62; 7.39, 5.91, 8.77 μM corresponding to the observed and estimated potencies, fit values = 9.98, 10.08, 9.91, respectively). The mild potent agent **33** exhibits the minimal error value (IC_{50} = 12.60, 11.14 μM corresponding to the observed and estimated potencies, respectively; error = 1.46, fit value = 9.80). Slightly higher error values were observed due to the mild potent synthesized compounds **26** and **34** (IC_{50}= 19.52, 15.60; 28.28, 30.73 μM corresponding to the observed and estimated potencies with error values = -8.76, -15.13, fit values = 9.40, 9.36, respectively). Compounds **20, 23, 25, 31** and **36** which are considered low effective agents reveal estimated potencies relatively consistent with their observed ones (IC_{50} = 26.10, 25.60, 22.62, 25.65, 28.60; 16.57, 39.34, 25.66, 30.87, 17.27 μM corresponding to the observed and estimated potencies, respectively with error value range = 3.04-13.74, fit value range = 9.26-9.63). However, compounds **24, 27** and **30** which are also considered low effective agents, reveal higher estimated potencies slightly deviated to their experimentally observed ones (IC_{50} = 36.21, 29.56, 29.60; 12.17, 11.53, 61.61 μM corresponding to the observed and estimated potencies, fit values = 9.77, 9.79, 9.06, respectively). Generally, the present pharmacophore seems more specific for estimating high potent than mild or low potent agents against LuPiCi carcinoma cell line.

All the synthesized spiro-alkaloids **20-36** are symmetrically mapped in the LuCa pharmacophore where, the indanyl and indolyl carbonyls are aligned with HBA-1, HBA-2, respectively, the aryl group attached to the pyrrolidinyl *C*-4' and benzonide residue of the indanyl function are aligned with H-1 and H-2, respectively and the cylclicamino *N*-1 is aligned with PosIon (Figure S3 of supporting information). Compounds **21, 22** and **29** which are considered high potent agents against LuCa carcinoma cell line reveal estimated bio-activities consistent with their lead potencies among the other synthesized analogues (IC_{50} = 2.70, 1.15, 2.62; 4.08, 2.96, 7.73 μM corresponding to the observed and estimated potencies, fit values = 9.81, 9.95, 9.54, respectively). The mild potent agents against LuCa cell line **27, 31** and **33** also reveal estimated bio-properties consistent with their observed activities (IC_{50} = 13.62, 11.62, 8.62; 9.16, 14.82, 11.65 μM corresponding to the observed and estimated potencies,

fit value = 9.46, 9.25, 9.36, respectively). However, deviation is observed due to compound **30** which is considered a mild antitumor agent against LuCa cell line (IC_{50} = 13.62, 45.47 μM corresponding to the observed and estimated potencies, respectively, fit value = 8.77). The low antitumor agents against LuCa cell lines **23, 25, 28, 34** and **36** (observed IC_{50} = 15.60-22.20 μM) exhibit estimated bio-properties (IC_{50} = 14.61-27.63 μM, fit value range = 8.98-9.26). Compounds **20, 24** and **26** which are considered mild antitumor agents against LuCa cell line (observed IC_{50} = 21.60, 26.61 and 15.62 μM, respectively) reveal deviation due to their estimated activities (estimated IC_{50} = 10.95, 4.88, 8.39 μM, fit values = 9.38, 9.74, 9.50, respectively). From all the above it is obvious that the LuCa pharmacophore seems more specific for estimating high potent than mild or low potent bio-active agents.

2D-QSAR study

Data set

QSAR is capable to generate a relationship between the chemical structure of an organic compound and its physico-chemical properties. All the synthesized compounds **20-38** were used as a training set in the present QSAR study (short homogenous data set dealing with only one chemical scaffold). Attempts were made to enrich the data set used with external data points previously reported in the literature (chemically and pharmacologically similar to the present spiro-alkaloids) but were unsuccessful due to the limitation in the reports mentioning the present subject. The QSAR study was undertaken using comprehensive descriptors for structural and statistical analysis (CODESSA-Pro) software.

Methodology

Geometry of the training set compounds was optimized using molecular mechanics force field (MM^+) followed by the semi-empirical AM1 method implemented in the HyperChem 8.0 package. The structures were fully optimized without fixing any

Table 1 Antitumor properties of the spiro-alkaloids **20-38**.

Entry	Compd.	R	X	IC_{50} (μM)*		
				GaLa	LuPiCi	LuCa
1	**20**	Ph	CH_2	38.16 ± 1.23	26.10 ± 0.94	21.60 ± 0.78
2	**21**	Ph	O	8.01 ± 0.96	3.20 ± 0.52	2.70 ± 0.09
3	**22**	4-BrC_6H_4	CH_2	9.15 ± 0.84	2.92 ± 0.34	1.15 ± 0.12
4	**23**	4-ClC_6H_4	CH_2	32.69 ± 2.23	25.60 ± 1.05	15.60 ± 0.59
5	**24**	4-ClC_6H_4	O	51.01 ± 2.51	36.21 ± 1.12	26.61 ± 0.96
6	**25**	2,4-$Cl_2C_6H_3$	CH_2	32.15 ± 1.59	22.62 ± 0.94	19.62 ± 1.26
7	**26**	2,4-$Cl_2C_6H_3$	O	32.15 ± 1.59	19.52 ± 0.62	15.62 ± 0.58
8	**27**	4-$H_3CC_6H_4$	CH_2	42.60 ± 2.01	29.56 ± 0.96	13.62 ± 0.36
9	**28**	4-$H_3CC_6H_4$	O	52.08 ± 2.12	33.60 ± 2.12	22.20 ± 1.26
10	**29**	4-$H_3CC_6H_4$	NMe	5.50 ± 0.23	3.62 ± 0.32	2.62 ± 0.32
11	**30**	4-$H_3COC_6H_4$	CH_2	44.40 ± 2.01	29.60 ± 3.25	13.62 ± 1.05
12	**31**	4-$H_3COC_6H_4$	O	43.41 ± 1.95	25.65 ± 1.88	11.62 ± 1.12
13	**32**	3,4,5-$(H_3CO)_3C_6H_2$	CH_2	86.84 ± 5.25	53.60 ± 4.44	46.60 ± 3.15
14	**33**	3,4,5-$(H_3CO)_3C_6H_2$	O	45.55 ± 3.25	12.60 ± 1.02	8.62 ± 0.76
15	**34**	4-$(H_3C)_2NC_6H_4$	CH_2	28.12 ± 1.25	15.60 ± 1.11	15.75 ± 0.55
16	**35**	4-$(H_3C)_2NC_6H_4$	O	334.00 ± 17.05	313.50 ± 18.06	296.80 ± 14.40
17	**36**	2-Thienyl	CH_2	53.60 ± 0.85	28.60 ± 2.25	18.62 ± 0.74
18	**37**	2,4-$Cl_2C_6H_3$	--	5.04 ± 0.26	2.25 ± 0.09	1.36 ± 0.23
19	**38**	4-$(H_3C)_2NC_6H_4$	--	277.90 ± 12.6	312.20 ± 15.62	189.60 ± 11.12
20	**Doxorubicin**	--	--	2.15 ± 0.45	0.95 ± 0.11	0.76 ± 0.21

*IC50 = concentration required to produce 50% inhibition of cell growth compared to control experiment.

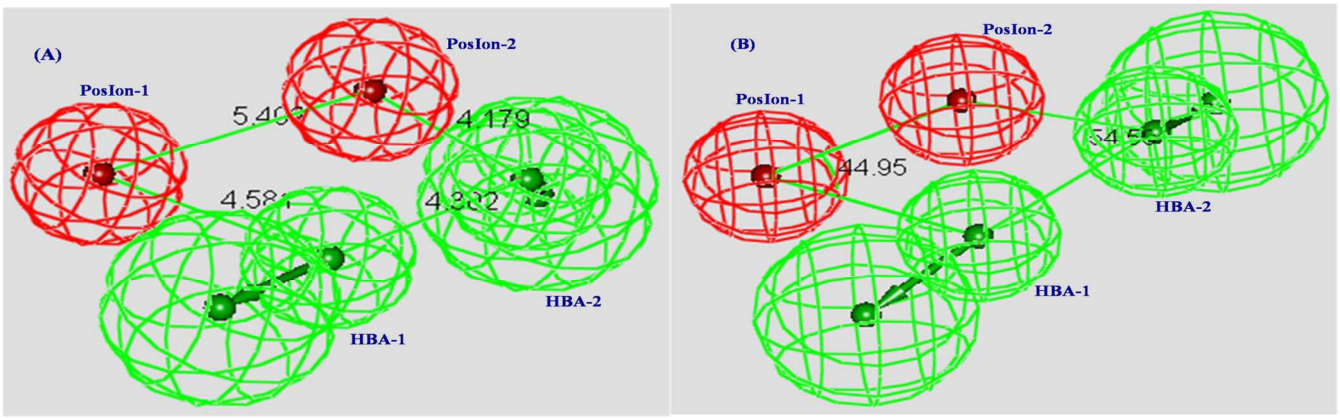

Figure 2 (**A**) Constraint distances and (**B**) constraint angles of the generated 3D-pharmacophore for the synthesized spiro-alkaloids **20-36** against GaLa cell line which contains two hydrogen bonding acceptors (HBA-1, HBA-2, green) and two positive ionizables (PosIon-1, PosIon-2, red).

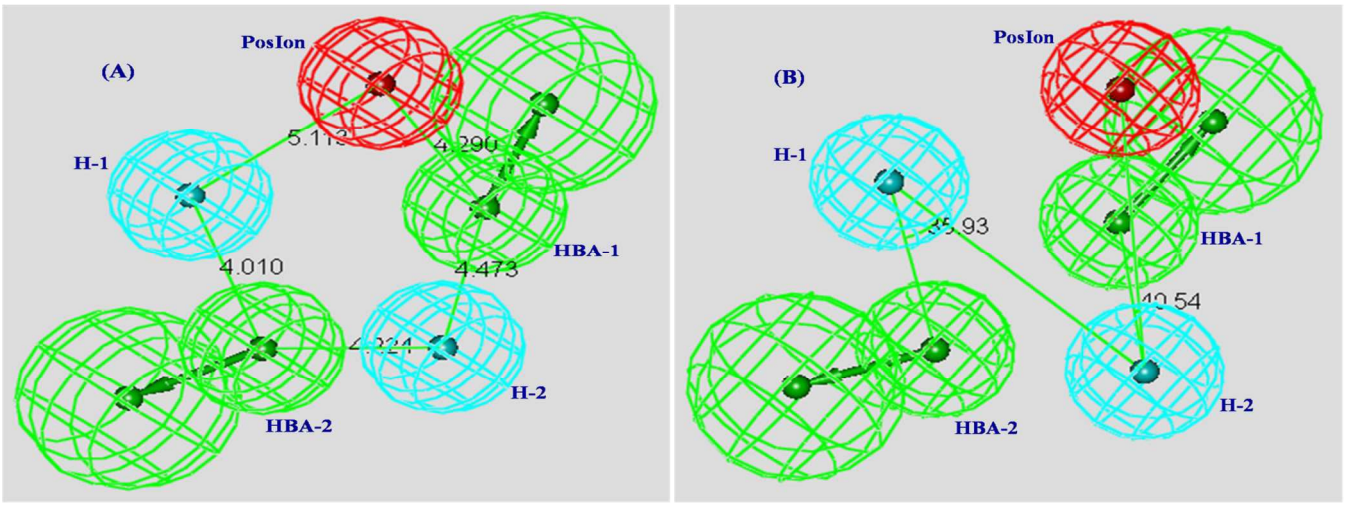

Figure 3 (**A**) Constraint distances and (**B**) constraint angles of the generated 3D-pharmacophore for the synthesized spiro-alkaloids **20-36** against LuPiCi cell line which contains two hydrogen bonding acceptors (HBA-1, HBA-2, green), two hydrophobics (H-1, H-2, light blue) and positive ionizable (PosIon, red).

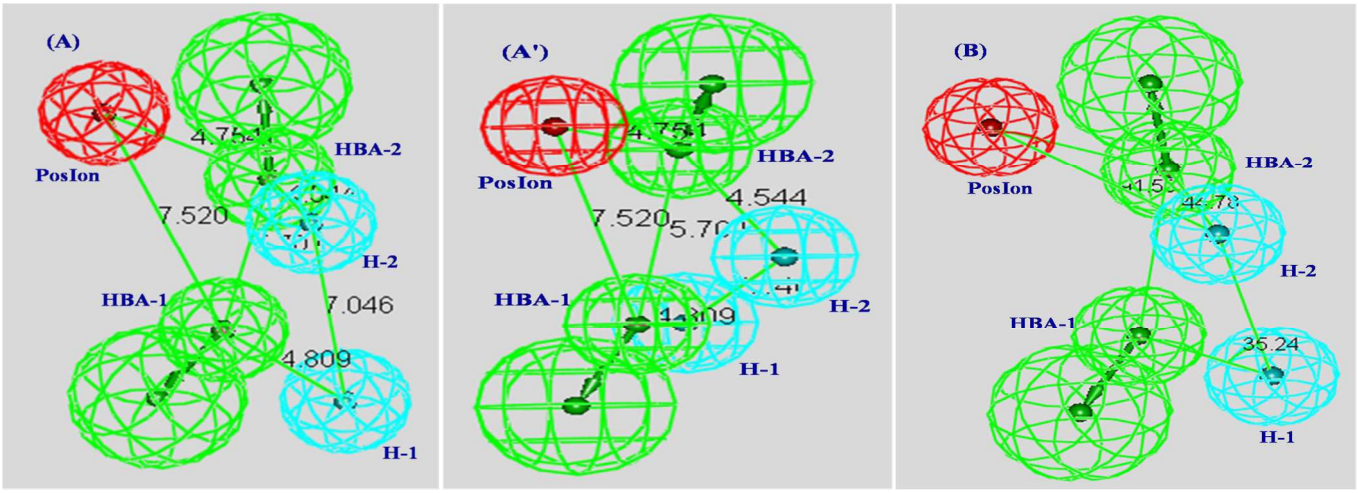

Figure 4 (**A, A'**) Constraint distances and (**B**) constraint angles of the generated 3D-pharmacophore for the synthesized spiro-alkaloids **20-36** against LuCa cell line which contains two hydrogen bonding acceptors (HBA-1, HBA-2, green), two hydrophobics (H-1, H-2, light blue) and positive ionizable (PosIon, red).

parameters, thus bringing all geometric variables to their equilibrium values. The energy minimization protocol employed the Polake-Ribiere conjugated gradient algorithm. Convergence to a local minimum was achieved when the energy gradient was ≤0.01 Kcal/mol. The RHF method was used in spin pairing for the two semi-empirical tools.[28,33,36-39] The resulting output files were exported to CODESSA-Pro that includes MOPAC capability for final geometry optimization. CODESSA-Pro software includes the following: (a) a calculation engine for more than 500 descriptors and (b) an engine for the development of the statistically most important linear and nonlinear QSAR regression models. CODESSA-Pro calculated 766 molecular descriptors including constitutional, topological, geometrical, charge-related, semi-empirical, thermodynamic, molecular-type, atomic-type and bond-type descriptors for the exported 19 bio-active spiro-alkaloids **20-38** which were used as a training set in the present study. Different mathematical transformations of the experimentally observed property/activity (IC_{50}, μM) against GaLa, LuPiCi and LuCa carcinoma cell lines of the training set compounds were utilized for the present QSAR modeling determination including property (IC_{50}, μM), 1/property, log(property) and 1/log(property) values in searching for the best QSAR models.

QSAR modeling

Best multi-linear regression (BMLR) was utilized which is a stepwise search for the best n-parameter regression equations (where, n stands for the number of descriptors used), based on the highest R^2 (squared correlation coefficient), R^2_{cv}OO (squared cross-validation "leave one-out, LOO" coefficient), R^2_{cv}MO (squared cross-validation "leave many-out, LMO" coefficient), F (Fisher statistical significance criteria) values, and s^2 (standard deviation). The QSAR models up to 3 descriptor models describing bio-activity of the antitumor active agents against

Table 2 Best fit values and estimated/predicted activities for the synthesized spiro-alkaloids **20-36** mapped with the generated 3D-pharmacophore models due to GaLa, LuPiCi and LuCa cancinoma cell lines.

Entry	Compd.	GaLa cell line			LuPiCi cell line			LuCa cell line		
		Observed IC_{50}, μM	Estimated IC_{50}, μM	Fit value	Observed IC_{50}, μM	Estimated IC_{50}, μM	Fit value	Observed IC_{50}, μM	Estimated IC_{50}, μM	Fit value
1	**20**	38.16	33.22	6.97	26.10	16.57	9.63	21.60	10.95	9.38
2	**21**	8.01	23.43	7.12	3.20	7.39	9.98	2.70	4.08	9.81
3	**22**	9.15	23.45	7.12	2.92	5.91	10.08	1.15	2.96	9.95
4	**23**	32.69	25.52	7.09	25.60	39.34	9.26	15.60	21.16	9.10
5	**24**	51.01	52.38	6.77	36.21	12.17	9.77	26.61	4.88	9.74
6	**25**	32.15	23.48	7.12	22.62	25.66	9.44	19.62	19.13	9.14
7	**26**	32.15	30.26	7.01	19.52	28.28	9.40	15.62	8.39	9.50
8	**27**	42.60	31.67	6.99	29.56	11.53	9.79	13.62	9.16	9.46
9	**28**	52.08	36.95	6.93	33.60	12.20	9.77	22.20	25.14	9.02
10	**29**	5.50	4.75	7.82	3.62	8.77	9.91	2.62	7.73	9.54
11	**30**	44.40	68.28	6.66	29.60	61.61	9.06	13.62	45.47	8.77
12	**31**	43.41	49.83	6.80	25.65	30.87	9.36	11.62	14.82	9.25
13	**32**	86.84	38.11	6.91	53.60	55.93	9.10	46.60	48.84	8.74
14	**33**	45.55	90.76	6.54	12.60	11.14	9.80	8.62	11.65	9.36
15	**34**	28.12	33.07	6.97	15.60	30.73	9.36	15.75	27.63	8.98
16	**35**	334.00	104.05	6.48	313.50	80.61	8.95	296.80	55.43	8.68
17	**36**	53.60	41.37	6.88	28.60	17.27	9.61	18.62	14.61	9.26

GaLa, LuPiCi and LuCa carcinoma cell lines were generated (obeying the thumb rule of 5:1, which is the ratio between the data points and the number of QSAR descriptor models). Observed and predicated values of the training set compounds **20-38** according to the multi-linear QSAR models are presented in Table 3. The statistical characteristics of the best QSAR models attained are presented in Tables 4-6 (Tables S1-S3 and Figures S4-S6 of supporting information exhibit the two descriptor QSAR models of the GaLa, LuPiCi and LuCa cell lines). The established QSAR models are statistically significant. The descriptors are sorted in descending order of the respective values of the Student's t-criterion, which is a widely accepted measure of statistical significance of individual parameters in multiple linear regressions. Figures 5-7 exhibit the QSAR multi-linear models plot of correlations representing the observed *vs.* predicted log(IC_{50}) values for GaLa, LuPiCi and LuCa tumor cell line active agents. The scattered plots are uniformly distributed, covering ranges, observed 0.702-2.524, 0.352-2.496, 0607-2.47; predicted 0.636-2.323, 0.314-2.268, 0.061-2.268 logarithmic units for GaLa, LuPiCi and LuCa cell lines, respectively.

Molecular Descriptors

Molecular descriptors are the physico-chemical parameters used to correlate chemical structure and property value expressed as log(IC_{50}). The descriptors were obtained based on BMLR method. The descriptors controlling the bio-activity (property) by the established multi-linear QSAR models are presented in Tables 4-6 and are arranged, based on their level of significance (t-criterion).

GaLa carcinoma cell line

The descriptors controlling bio-activity of the synthesized compounds against GaLa carcinoma cell line according to the attained 3 descriptor QSAR model (Table 4) are: minimum total interaction for bond C-N, maximum SIGMA-SIGMA bond order, and RPCS relative positive charged SA (SAMPOS*RPCG) (Zefirov PC). The first descriptor controlling the GaLa-QSAR model is minimum total interaction for bond C-N (t = 6.078) is a semi-empirical descriptor. Maximum σ - σ bond order which is the second descriptor controlling the GaLa-QSAR model (t = -5.260) is also a semi-empirical descriptor related to the strength of intramolecular bonding interactions and characterizes the stability of the molecule, conformational flexibility and other valency-related properties for a given pair of atomic species in the molecule.[40] Relative positive charged SA (SAMPOS*RPCG) (Zefirov PC) which is the third descriptor controlling the GaLa-QSAR model (t = -5.670) is a charge-related descriptor. Relative positive charge encodes the influence of the high positively charged atom on the overall charge of the molecule. Partial positively charged surface area is determined by equation (1).[41]

$$PPSA1 = \sum_A S_A \quad \text{..... (1)}$$

where, S_A stands for the positively charged solvent-accessible atomic surface area.

LuPiCi carcinoma cell line

Descriptors controlling the LuPiCi carcinoma cell line are the same of the previously mentioned GaLa carcinoma cell line with the same order of importance based on their t-criterion values but with different coefficient values determining the log(IC_{50}) "potency" values (Table 5). This observation supports the assumption that the major structural factors affecting the potency of the synthesized compounds are the same in case of the two mentioned tumor cell lines and are related to their basic skeleton (scaffold) as explained in the 3D-pharmacophore modeling studies (three common features "two HBA and one PosIon" correlated to the indanyl and indolyl carbonyls, and cyclicamino functions were revealed in both GaLa and LuPiCi 3D-pharmacophore models).

LuCa carcinoma cell line

The first descriptor controlling the LuCa carcinoma cell line is relative number of Br atoms based on its superior t-criterion value among the other descriptors controlling the QSAR model (t = -3.279). Number of Br atoms is a constitutional descriptor characterizing the atomic composition and also polarizability. The number of Br atoms also serves as an indicator variable to distinguish between the only bromine-containing compound (the most active synthesized agent **22**, IC_{50} = 1.15 μM) and the rest of the LuCa training set agents. This descriptor has the greatest influence on the QSAR model due to its highest negative coefficient value (-80.286) relative to the other descriptors controlling the model, affecting greatly the potency of the bromine bearing-compounds. Charged surface area for atom N which is the second descriptor controlling the LuCa-QSAR model (t = -3.517), is a charge-related descriptor. Surface weighted charged partial positive charged surface area is determined by equation (2).[41]

$$WPSA1=\frac{PPSA1-TMSA}{1000} \quad \ldots\ldots\ldots\ldots\ldots\ldots\ldots\ldots\ldots\ldots \quad (2)$$

where, PPSA1 stands for partial positively charged molecular surface area and TMSA for total molecular surface area. The present descriptor has the minimal coefficient value among all the other LuCa-QSAR model descriptors (coefficient = -0.994). HOMO-LUMO energy gap is the third descriptor controlling the attained model (t = -5.695) which is a semi-empirical descriptor. Highest occupied molecular orbital (HOMO) energy and lowest unoccupied molecular orbital (LUMO) energy are determined by equations (3, 4).[41]

$$\varepsilon_{HOMO}=\langle \phi_{HOMO} | \hat{\mathbf{F}} | \phi_{HOMO} \rangle \quad \ldots\ldots\ldots\ldots\ldots\ldots \quad (3)$$

$$\varepsilon_{LUMO}=\langle \phi_{LUMO} | \hat{\mathbf{F}} | \phi_{LUMO} \rangle \quad \ldots\ldots\ldots\ldots\ldots\ldots \quad (4)$$

where, ϕ_{HOMO} stands for highest occupied molecular orbital and ϕ_{LUMO} lowest unoccupied molecular orbital. The large HOMO-LUMO gaps infer good stability, high excitation energies for many of the excited states, and large chemical hardness of the molecules.[37] The present descriptor participates negatively in the LuCa-QSAR model (coefficient = -2.304) meaning that the high HOMO-LUMO energy gap, the high pharmacologically potent analogue against the LuCa carcinoma cell line.

Molecular descriptor values controlling the attained QSAR models are presented in Table S4 of supporting information. 2D-QSAR study was also undertaken utilizing average IC_{50} activity values of the three cell lines measured, obeying the same CODESSA-Pro protocol described. A statistically significant three descriptor model was obtained (N=19, n=3, R^2=0.799, R^2cvOO=0.688, R^2cvMO=0.711, F=19.912, s^2=0.069). The three descriptors controlling the attained model are, min. total interaction for bond C-N, max. SIGMA-SIGMA bond order and RPCS relative positive charged SA (SAMPOS*RPCG) (Zefirov PC) which are the same of GaLa and LuPiCi cell lines. These observations explain the importance of these parameters controlling the observed bio-properties (Tables S5, S6 and Figure S7 of supporting information).

Validation of QSAR models

The reliability and statistical relevance of the QSAR models are examined by internal validation procedures. The dataset contains relatively few experimental data points but is homogeneous. Therefore application of internal validation methodology is an appropriate technique.[26] Internal validation is applied by the CODESSA-Pro technique employing both leave one out (LOO), which involves developing a number of models with one example omitted at a time, and leave many out (LMO), which involves developing number of models with many data points omitted at a time (up to 20% of the total data points). The observed correlations due to the internal validation techniques are R^2cvOO = 0.724, 0.676, 0.615; R^2_{cv}MO = 0.728, 0.688, 0.782 for GaLa, LuPiCi and LuCa QSAR models, respectively. All of them are significantly correlated with the squared correlation coefficient of the attained QSAR models (R^2 = 0.813, 0.803, 0.750 for GaLa, LuPiCi and LuCa QSAR models, respectively). Standard deviation of the regressions (s^2 = 0.052, 0.080, 0.113 for GaLa, LuPiCi and LuCa QSAR models, respectively) is also a measurable value for the attained model together with the Fisher test value (F = 21.670, 20.330, 15.015 for GaLa, LuPiCi and LuCa QSAR models, respectively) that reflects the ratio of the variance explained by the model and the variance due to their errors. A high value of F-test relative to the s^2 value is also validation of the model.

The estimated/predicted IC_{50} values of compounds **22, 29** and **37** which are considered high potent analogues among all the training set compounds against GaLa carcinoma cell line, are correlated with their observed ones (IC_{50} observed = 9.15, 5.50, 5.04 μM, IC_{50} estimated = 8.97, 4.33, 9.57 μM, error "difference between observed and estimated values" = 0.18, 1.17, -4.53 for compounds **22, 29** and **37**, respectively). Compounds **21** which is also considered a high potent agent against GaLa cell line, reveals estimated potency slightly deviated from its observed bio-activity (IC_{50} observed = 8.01 μM, IC_{50} estimated = 18.37 μM, error = -10.36). This observation is also exhibited by compound **21** during 3D-pharmacophore modeling studies (IC_{50} = 8.01, 23.43 μM corresponding to the observed and estimated values, respectively). The mild antitumor agents against GaLa cell line **20, 23, 25, 26** and **34** (IC_{50} observed = 28.12-38.16 μM) reveal compatible estimated bio-properties (IC_{50} estimated = 21.32-36.47 μM). Similar observations are shown by most of the low antitumor active agents against GaLa cell line **24, 27, 28, 31, 33** and **36** (IC_{50} = 42.60-53.60, 23.32-50.42 μM corresponding to the observed and estimated values, respectively). Additionally, the very low antitumor agents against GaLa cell line (practically inactive agents) **32, 35** and **38** are also controlled by the attained QSAR model (IC_{50} = 86.84, 334.00, 277.90; 115.55, 152.18, 210.41 μM corresponding to the observed and estimated values, respectively).

The LuPiCi-QSAR model reveals estimated bio-potencies due to all the high effective agents correlated with their observed ones (IC_{50} = 3.20, 2.92, 3.62, 2.25; 8.99, 3.65, 2.06, 4.36 μM corresponding to the observed and estimated values of compounds **21, 22, 29** and **37**, respectively). The same observations are shown by the mild antitumor agents **26, 33** and **34** (IC_{50} = 19.52, 12.60, 15.60; 16.14, 12.23, 17.21 μM

corresponding to the observed and estimated values, respectively). The LuPiCi-QSAR model is also applicable for most of the low antitumor active agents (IC_{50} = 25.60, 36.21, 29.56, 33.60, 25.65, 28.60; 20.44, 25.40, 29.69, 37.54, 32.57, 27.72 μM corresponding to the observed and estimated values of compounds **23, 24, 27, 28, 31** and **36**, respectively) and the very low antitumor agents "practically inactive agents" (IC_{50} = 53.60, 313.50, 312.20; 89.18, 114.89, 185.35 μM corresponding to the observed and estimated values of compounds **32, 35** and **38**, respectively).

The estimated bio-properties of the highly effective agents against LuCa carcinoma cell line are comparable with their observed values based on the attained QSAR model (IC_{50} = 2.70, 1.15, 2.62, 1.36; 8.02, 1.15, 1.59, 3.35 μM corresponding to the

Table 3 Observed and estimated/predicated values of the training set compounds **20-38** according to the BMLR-QSAR models.

Entry	Compd.	GaLa cell line			LuPiCi cell line			LuCa cell line		
		Observed IC_{50}, μM	Estimated IC_{50}, μM	Error	Observed IC_{50}, μM	Estimated IC_{50}, μM	Error	Observed IC_{50}, μM	Estimated IC_{50}, μM	Error
1	**20**	38.16	27.81	10.35	26.10	14.59	11.51	21.60	9.85	11.75
2	**21**	8.01	18.37	-10.36	3.20	8.99	-5.79	2.70	8.02	-5.32
3	**22**	9.15	8.97	0.18	2.92	3.65	-0.73	1.15	1.15	0.00
4	**23**	32.69	36.47	-3.78	25.60	20.44	5.16	15.60	14.59	1.01
5	**24**	51.01	43.73	7.28	36.21	25.40	10.81	26.61	30.93	-4.32
6	**25**	32.15	21.32	10.83	22.62	10.97	11.65	19.62	19.93	-0.31
7	**26**	32.15	29.43	2.72	19.52	16.14	3.38	15.62	22.99	-7.37
8	**27**	42.60	40.55	2.05	29.56	29.69	-0.13	13.62	20.44	-6.82
9	**28**	52.08	49.71	2.37	33.60	37.54	-3.94	22.20	20.60	1.60
10	**29**	5.50	4.33	1.17	3.62	2.06	1.56	2.62	1.59	1.03
11	**30**	44.40	142.95	-98.55	29.60	113.75	-84.15	13.62	27.17	-13.55
12	**31**	43.41	50.42	-7.01	25.65	32.57	-6.92	11.62	8.36	3.26
13	**32**	86.84	115.55	-28.71	53.60	89.18	-35.58	46.60	17.40	29.20
14	**33**	45.55	23.32	22.23	12.60	12.23	0.37	8.62	11.52	-2.90
15	**34**	28.12	30.88	-2.76	15.60	17.21	-1.61	15.75	50.31	-34.56
16	**35**	334.00	152.18	181.83	313.50	114.89	198.61	296.80	74.52	222.28
17	**36**	53.60	42.98	10.62	28.60	27.72	0.88	18.62	7.22	11.40
18	**37**	5.04	9.57	-4.53	2.25	4.36	-2.11	1.36	3.35	-1.99
19	**38**	277.90	210.41	67.49	312.20	185.35	126.84	189.60	185.19	4.41

Table 4 Descriptor of the BMLR-QSAR model for the GaLa carcinoma cell line active agents.

N=19, n=3, R^2=0.813, R^2_{cv}OO=0.724, R^2_{cv}MO=0.728, F=21.670, s^2=0.052					
Entry	ID	coefficient	s	t	Descriptor
1	0	91.220	37.072	2.461	Intercept
2	D_1	6.946	1.143	6.078	Min. total interaction for bond C-N
3	D_2	-195.124	37.093	-5.260	Max. SIGMA-SIGMA bond order
4	D_3	-6.499	1.146	-5.670	RPCS Relative positive charged SA (SAMPOS*RPCG) (Zefirov PC)
$\log(IC_{50}) = 91.220 + (6.946 \times D_1) - (195.124 \times D_2) - (6.499 \times D_3)$					

Table 5 Descriptor of the BMLR-QSAR model for the LuPiCi carcinoma cell line active agents.

N=19, n=3, R^2=0.803, R^2_{cv}OO=0.676, R^2_{cv}MO=0.688, F=20.330, s^2=0.080					
Entry	ID	coefficient	S	t	Descriptor
1	0	84.672	45.975	1.842	Intercept
2	D_1	8.635	1.417	6.093	Min. total interaction for bond C-N
3	D_2	-213.575	46.001	-4.643	Max. SIGMA-SIGMA bond order
4	D_3	-7.984	1.421	-5.617	RPCS Relative positive charged SA (SAMPOS*RPCG) (Zefirov PC)
$\log(IC_{50}) = 84.672 + (8.635 \times D_1) - (213.575 \times D_2) - (7.984 \times D_3)$					

Table 6 Descriptor of the BMLR-QSAR model for the LuCa carcinoma cell line active agents.

N=19, n=3, R^2=0.750, R^2_{cv}OO=0.615, R^2_{cv}MO=0.782, F=15.015, s^2=0.113					
Entry	ID	coefficient	s	t	Descriptor
1	0	21.033	3.460	6.079	Intercept
2	D_1	-80.286	24.488	-3.279	Relative number of Br atoms
3	D_2	-0.994	0.283	-3.517	Charged surface area for atom N
4	D_3	-2.304	0.405	-5.695	HOMO-LUMO energy gap
$\log(IC_{50}) = 21.033 - (80.286 \times D_1) - (0.994 \times D_2) - (2.304 \times D_3)$					

Organic &Biomolecular Chemistry RSCPublishing

PAPER

observed and estimated values of compounds **21, 22, 29** and **37**, respectively). Most of the mild antitumor agents against LuCa cell line also reveal similar behavior (IC_{50} = 11.62, 8.62; 8.36, 11.52 μM corresponding to the observed and estimated values of compounds **31** and **33**, respectively). Slight deviation is observed for the mild antitumor agents against LuCa cell line by compounds **27** and **30** (IC_{50} = 13.62; 20.44, 27.17 μM corresponding to the observed and estimated values, respectively). The LuCa-QSAR model exhibits controlled bio-properties for the most low antitumor agents **23-26** and **28** (IC_{50} = 15.60-26.61, 14.59-30.93 corresponding to the observed and estimated values, respectively) and the very low antitumor agents "practically inactive agents" **35** and **38** (IC_{50} = 296.80, 189.60; 74.52, 185.19 corresponding to the observed and estimated values, respectively). The overall observations due to different validation procedures/techniques of GaLa, LuPiCi and LuCa-QSAR models give good indications for their predictive ability for optimizing promising hits of spiro-alkaloid scaffold.

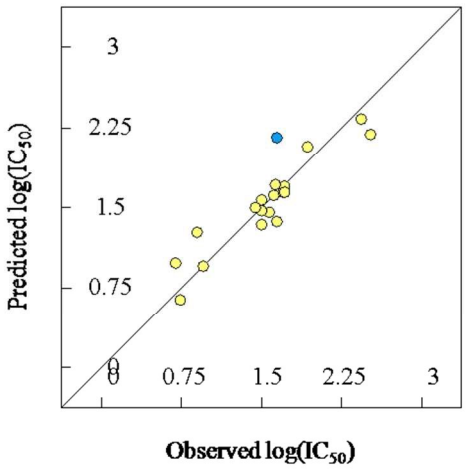

Figure 5 BMLR-QSAR model plot of correlations representing the observed *vs.* predicted log(IC_{50}) values for GaLa carcinoma cell line active agents (compound **30** is an outlier).

Conclusion

In conclusion, dispiro[2*H*-indene-2,3'-pyrrolidine-2',3"-[3*H*]indole]-1,2"(1"*H*, 3*H*)-diones **20-38** were prepared *via* 1,3-dipolar cycloaddition reactions of azomethine ylides, (generated *in situ via* decarboxylative condensation of isatin derivatives **7-9** with sarcosine **10**) and 2-(arylmethylidene)-2,3-dihydro-1*H*-inden-1-ones **11-19** in refluxing ethanol. Some of the newly synthesized compounds, **21, 22, 29** and **37** reveal promising antitumor properties against GaLa, LuPiCi and LuCa carcinoma

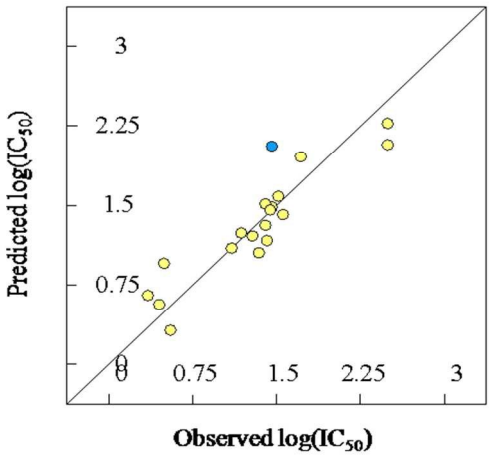

Figure 6 BMLR-QSAR model plot of correlations representing the observed *vs.* predicted log(IC_{50}) values for LuPiCi carcinoma cell line active agents (compound **30** is an outlier).

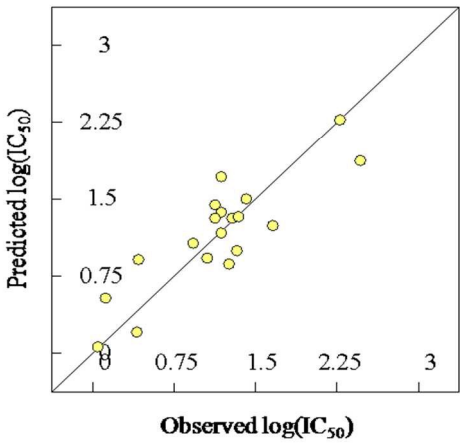

Figure 7 BMLR-QSAR model plot of correlations representing the observed *vs.* predicted log(IC_{50}) values for LuCa carcinoma cell line active agents.

cell lines with potency close to that of the standard reference doxorubicin through *in vitro* Sulfo-Rhodamine-B standard method. The use of Discovery Studio 2.5 and CODESSA-PRO software provided robust 3D-pharmacophores and 2D-QSAR models describing the bio-properties of the antitumor active spiro-alkaloids. The observed computational models are statistically significant based on the cross validation, and potency difference between the experimentally observed and predicted values. Although the present computational studies make use a short size dataset, homogeneity of the set analogues (the same scaffold) may be the main factor contributing to the satisfactory agreement between experimental (observed) and estimated

results. Applicability of these models can be used for predication of more highly effective hits in a future studies.

Experimental section

Melting points were determined on an Electrothermal Stuart SMP3 melting point apparatus. IR spectra (KBr) were recorded on a JASCO 6100 spectrophotometer. ^{1}H-NMR spectra were recorded on Varian MERCURY 300 (^{1}H: 300 MHz) and JEOL AS 500 (^{1}H: 500 MHz) spectrometers. ^{13}C-NMR spectra were recorded on a JEOL AS 500 (^{13}C: 125 MHz) spectrometer. HRMS were recorded on Agilent Technology 6210 Time of Flight LC/MS spectrometer operating in the ESI mode. Compounds **7-9**[42,43] and **11-19**[44-48] were prepared according to reported procedures.

Synthesis of dispiro[2*H*-indene-2,3'-pyrrolidine-2',3''-[3*H*]indole]-1,2''(1''*H*, 3*H*)-dione 20-38 (general procedure)

Equimolar quantities of 2-(arylmethylidene)-2,3-dihydro-1*H*-inden-1-ones **11-19** (5 mmol), the appropriate isatin **7-9** and sarcosine **10** were heated under reflux for the specified time in ethanol (25 ml). The separated solid was collected and crystallized from a suitable solvent affording the corresponding **36**. For the preparation of compounds **20, 22, 23, 25, 26, 28, 30** and **32-35**, the reaction mixtures were stored at 20 °C overnight. The separated solids were collected and crystallized from suitable solvents. In the cases of compounds **21, 24, 27, 29** and **31** each reaction mixture was evaporated to dryness. Each residue was triturated with methanol (5 ml) and the separated solid was collected and crystallized from a suitable solvent. On heating **14** or **18** with **9** under the previously described procedure, **37** and **38** were isolated.

1'-Methyl-4'-phenyl-1''-[(1-piperidinyl)methylene]-dispiro[2*H*-indene-2,3'-pyrrolidine-2',3''-[3*H*]indole]-1,2''(1''*H*, 3*H*)-dione (20)

Obtained from reaction of **11**, **7** and **10**. Reaction time 15 h, colorless microcrystals from *n*-butanol, m.p. 179-181 °C, yield (1.30 g) 53%. IR ν (cm^{-1}): 1707, 1607, 1488. ^{1}H-NMR (500 MHz, $CDCl_3$) δ (ppm): 1.33-1.53 (m, 6H), 2.15 (s, 3H), 2.38 (br d, 4H), 2.69 (d, J = 17.6 Hz, 1H), 3.11 (d, J = 18.4 Hz, 1H), 3.57 (t, J = 8.8 Hz, 1H), 4.07 (t, J = 9.6 Hz, 1H), 4.16 (d, J = 12.2 Hz 1H), 4.36-4.45 (m, 2H), 6.74-7.45 (m, 13H). ^{13}C-NMR (125 MHz, $CDCl_3$) δ (ppm): 24.1, 25.9, 35.3, 35.4, 49.8, 52.0, 59.1, 62.8, 66.9, 78.8, 109.4, 122.7, 123.9, 125.2, 125.4, 127.1, 127.2, 127.3, 128.5, 129.2, 130.1, 134.5, 135.9, 139.3, 144.3, 151.7, 177.3, 206.4. Elemental analysis: $C_{32}H_{33}N_3O_2$ required C, 78.18; H, 6.77; N, 8.55, found C, 78.10; H, 7.09; N, 8.33.

1'-Methyl-1''-[(4-morpholinyl)methylene]-4'-phenyl-dispiro[2*H*-indene-2,3'-pyrrolidine-2',3''-[3*H*]indole]-1,2''(1''*H*, 3*H*)-dione (21)

Obtained from reaction of **11**, **8** and **10**. Reaction time 13 h, colorless microcrystals from *n*-butanol, m.p. 183-185 °C, yield (1.50 g) 61%. IR ν (cm^{-1}): 1722, 1705, 1604, 1451. ^{1}H-NMR (500 MHz, $CDCl_3$) δ (ppm): 2.16 (s, 3H), 2.38-2.47 (m, 4H), 2.70 (d, J = 17.6 Hz, 1H), 3.11 (d, J = 17.6 Hz, 1H), 3.59-3.61 (m, 5H), 4.07 (t, J = 9.2 Hz, 1H), 4.21 (d, J = 12.3 Hz, 1H), 4.40-4.47 (m, 2H), 6.70-7.50 (m, 13H). ^{13}C-NMR (125 MHz, $CDCl_3$) δ (ppm): 35.2, 35.5, 49.7, 51.0, 59.0, 62.1, 66.8, 67.0, 78.3, 109.2, 122.9, 124.0, 125.2, 125.5, 127.1, 127.4, 127.8, 128.6, 129.2, 130.1, 134.6, 135.9, 139.2, 143.8, 151.6, 177.3, 206.2. Elemental analysis: $C_{31}H_{31}N_3O_3$ required C, 75.43; H, 6.33; N, 8.51, found C, 75.66; H, 6.59; N, 8.58.

4'-(4-Bromophenyl)-1'-methyl-1''-[(1-piperidinyl)methylene]-dispiro[2*H*-indene-2,3'-pyrrolidine-2',3''-[3*H*]indole]-1,2''(1''*H*, 3*H*)-dione (22)

Obtained from reaction of **12**, **7** and **10**. Reaction time 2 h, colorless microcrystals from ethanol, m.p. 147-149 °C, yield (2.00 g) 70%. IR ν (cm^{-1}): 1722, 1709, 1604, 1465. ^{1}H-NMR (500 MHz, $CDCl_3$) δ (ppm): 1.37 (br s, 2H), 1.51 (t, J = 5.35 Hz, 4H), 2.15 (s, 3H), 2.42 (br d, 4H), 2.65 (d, J = 18.4 Hz, 1H), 3.05 (d, J = 17.6 Hz, 1H), 3.60 (t, J = 8.8 Hz, 1H), 4.01 (t, J = 9.2 Hz, 1H), 4.19 (d, J = 13.0 Hz, 1H), 4.36 (t, J = 8.8 Hz, 1H), 4.44 (d, J = 13.0 Hz, 1H), 6.76-7.50 (m, 12H). ^{13}C-NMR (125 MHz, $CDCl_3$) δ (ppm): 24.0, 25.8, 35.4, 49.3, 52.1, 59.2, 62.8, 66.5, 78.2, 109.5, 121.1, 122.8, 124.1, 124.9, 125.4, 127.2, 127.5, 129.3, 131.6, 132.0, 134.7, 135.8, 138.5, 144.3, 151.4, 177.4, 206.4. Elemental analysis: $C_{32}H_{32}BrN_3O_2$ required C, 67.37; H, 5.65; N, 7.37, found C, 67.09; H, 5.74; N, 7.03.

4'-(4-Chlorophenyl)-1'-methyl-1''-[(1-piperidinyl)methylene]-dispiro[2*H*-indene-2,3'-pyrrolidine-2',3''-[3*H*]indole]-1,2''(1''*H*, 3*H*)-dione (23)

Obtained from reaction of **13**, **7** and **10**. Reaction time 15 h, colorless microcrystals from ethanol, m.p. 140-142 °C, yield (1.40 g) 53%. IR ν (cm^{-1}): 1723, 1703, 1604, 1464. ^{1}H-NMR (500 MZ, $CDCl_3$) δ (ppm): 1.34 (br s, 2H), 1.48 (br s, 4H), 2.13 (s, 3H), 2.40 (br d, 4H), 2.63 (d, J = 17.6 Hz, 1H), 3.04 (d, J = 17.6 Hz, 1H), 3.57 (t, J = 8.4 Hz, 1H), 4.00 (t, J = 9.2 Hz, 1H), 4.17 (d, J = 13.0 Hz, 1H), 4.34-4.43 (m, 2H), 6.74-7.46 (m, 12H). ^{13}C-NMR (125 MHz, $CDCl_3$) δ (ppm): 24.1, 25.8, 35.3, 49.2, 52.1, 59.2, 62.8, 66.6, 78.2, 109.5, 122.7, 124.0, 124.9, 125.4, 127.1, 127.4, 128.7, 129.2, 131.5, 132.9, 134.7, 135.8, 137.9, 144.3, 151.4, 177.3, 206.4. Elemental analysis: $C_{32}H_{32}ClN_3O_2$ required C, 73.06; H, 6.13; N, 7.99, found C, 72.73; H, 6.34; N, 7.73.

4'-(4-Chlorophenyl)-1'-methyl-1''-[(4-morpholinyl)methylene]-dispiro[2*H*-indene-2,3'-pyrrolidine-2',3''-[3*H*]indole]-1,2''(1''*H*, 3*H*)-dione (24)

Obtained from reaction of **13**, **8** and **10**. Reaction time 12 h, colorless microcrystals from ethanol, m.p. 175-177 °C, yield (1.45 g) 55%. IR ν (cm^{-1}): 1715, 1604, 1465. ^{1}H-NMR (500 MHz, $CDCl_3$) δ (ppm): 2.16 (s, 3H), 2.41-2.50 (m, 4H), 2.66 (d, J = 17.6 Hz, 1H), 3.05 (d, J = 18.4 Hz, 1H), 3.58-3.63 (m, 5H), 4.01 (t, J = 9.2 Hz, 1H), 4.23 (d, J = 13.0 Hz, 1H), 4.39-4.43 (m, 2H), 6.73-7.47 (m, 12H). ^{13}C-NMR (125 MHz, $CDCl_3$) δ (ppm): 35.2, 35.4, 49.2, 51.1, 59.1, 62.1, 66.7, 67.2, 78.2, 109.2, 123.0, 124.1, 125.0, 125.5, 127.5, 128.7, 129.3, 131.5, 132.9, 134.7, 135.8, 137.8, 143.8, 151.3, 177.3, 206.1. Elemental analysis:

$C_{31}H_{30}ClN_3O_3$ required C, 70.51; H, 5.73; N, 7.96, found C, 70.50; H, 5.84; N, 7.68.

4'-(2,4-Dichlorophenyl)-1'-methyl-1''-[(1-piperidinyl)methylene]-dispiro[2*H*-indene-2,3'-pyrrolidine-2',3''-[3*H*]indole]-1,2''(1''*H*, 3*H*)-dione (25)

Obtained from reaction of **14**, **7** and **10**. Reaction time 2 h, colorless microcrystals from ethanol, m.p. 125-127 °C, yield (1.55 g) 55%. IR ν (cm^{-1}): 1711, 1607, 1470. ^{1}H-NMR (300 MHz, $CDCl_3$) δ (ppm): 1.42-1.62 (m, 6H), 2.19 (s, 3H), 2.51 (t, J = 5.1 Hz, 4H), 2.57 (d, J = 18.3 Hz, 1H), 2.82 (d, J = 18.3 Hz, 1H), 3.64 (t, J = 8.6 Hz, 1H), 4.09 (t, J = 9.2 Hz, 1H), 4.24 (d, J = 12.6 Hz, 1H), 4.42 (d, J = 12.6 Hz, 1H), 4.90 (t, J = 8.9 Hz, 1H), 6.75-8.13 (m, 11H). Elemental analysis: $C_{32}H_{31}Cl_2N_3O_2$ required C, 68.57; H, 5.57; N, 7.50, found C, 68.29; H, 5.52; N, 7.46.

4'-(2,4-Dichlorophenyl)-1'-methyl-1''-[(4-morpholinyl)methylene]-dispiro[2*H*-indene-2,3'-pyrrolidine-2',3''-[3*H*]indole]-1,2''(1''*H*, 3*H*)-dione (26)

Obtained from reaction of **14**, **8** and **10**. Reaction time 2.5 h, colorless microcrystals from ethanol, m.p. 207-209 °C, yield (1.65 g) 59%. IR ν (cm^{-1}): 1711, 1606, 1469. ^{1}H-NMR (500 MHz, $CDCl_3$) δ (ppm): 2.17 (s, 3H), 2.22 (d, J = 17.6 Hz, 1H), 2.55 (br s, 4H), 2.75 (d, J = 17.6 Hz, 1H), 3.62-3.71 (m, 5H), 4.06 (t, J = 9.2 Hz, 1H), 4.30 (d, J = 13.0 Hz, 1H), 4.41 (d, J = 13.0 H, 1H), 4.86 (t, J = 8.8 Hz, 1H), 6.72-8.06 (m, 11H). Elemental analysis: $C_{31}H_{29}Cl_2N_3O_3$ required C, 66.19; H, 5.20; N, 7.47, found C, 66.13; H, 5.29; N, 7.12.

1'-Methyl-4'-(4-methylphenyl)-1''-[(1-piperidinyl)methylene]-dispiro[2*H*-indene-2,3'-pyrrolidine-2',3''-[3*H*]indole]-1,2''(1''*H*, 3*H*)-dione (27)

Obtained from reaction of **15**, **7** and **10**. Reaction time 10 h, colorless microcrystals from ethanol, m.p. 173-175 °C, yield (1.30 g) 51%. IR ν (cm^{-1}): 1722, 1604, 1462. ^{1}H-NMR (500 MHz, $CDCl_3$) δ (ppm): 1.35-1.49 (m, 6H), 2.16 (s, 3H), 2.27 (s, 3H), 2.40 (br d, 4H), 2.73 (d, J = 18.4 Hz, 1H), 3.13 (d, J = 17.6 Hz, 1H), 3.57 (t, J = 8.8 Hz, 1H), 4.06 (t, J = 9.6 Hz, 1H), 4.17 (d, J = 13.0 Hz, 1H), 4.41-4.46 (m, 2H), 6.75-7.47 (m, 12H). ^{13}C-NMR (125 MHz, $CDCl_3$) δ (ppm): 21.1, 24.0, 25.8, 35.2, 35.4, 49.4, 52.0, 59.1, 62.8, 66.9, 78.3, 109.4, 122.7, 123.9, 125.3, 125.5, 127.2, 129.1, 129.2, 130.0, 134.5, 136.0, 136.2, 136.6, 144.3, 151.8, 177.4, 206.6. Elemental analysis: $C_{33}H_{35}N_3O_2$ required C, 78.39; H, 6.98; N, 8.31, found C, 78.03; H, 7.39; N, 8.18.

1'-Methyl-4'-(4-methylphenyl)-1''-[(4-morpholinyl)methylene]-dispiro[2*H*-indene-2,3'-pyrrolidine-2',3''-[3*H*]indole]-1,2''(1''*H*, 3*H*)-dione (28)

Obtained from reaction of **15**, **8** and **10**. Reaction time 12 h, colorless microcrystals from *n*-butanol, m.p. 190-192 °C, yield (1.45 g) 57%. IR ν (cm^{-1}): 1726, 1706, 1604, 1513. ^{1}H-NMR (500 MHz, $CDCl_3$) δ (ppm): 2.17 (s, 3H), 2.28 (s, 3H), 2.37-2.48 (m, 4H), 2.73 (d, J = 17.6 Hz, 1H), 3.13 (d, J = 18.4 Hz, 1H), 3.58-3.61 (m, 5H), 4.06 (t, J = 9.6 Hz, 1H), 4.20 (d, J = 13.0 Hz, 1H), 4.41-4.46 (m, 2H), 6.73-7.48 (m, 12H). ^{13}C-NMR (125 MHz, $CDCl_3$) δ (ppm): 21.1, 35.1, 35.5, 49.3, 51.0, 59.0, 62.1, 66.8, 67.0, 78.3, 109.1, 122.9, 123.9, 125.2, 125.5, 127.3, 127.4, 129.3, 129.9, 134.5, 136.0, 136.7, 143.8, 151.7, 177.3, 206.3. Elemental analysis: $C_{32}H_{33}N_3O_3$ required C, 75.71; H, 6.55; N, 8.28, found C, 75.53; H, 6.84; N, 8.29.

1'-Methyl-4'-(4-methylphenyl)-1''-[(4-methylpiperazin-1-yl)methylene]-dispiro[2*H*-indene-2,3'-pyrrolidine-2',3''-[3*H*]indole]-1,2''(1''*H*, 3*H*)-dione (29)

Obtained from reaction of **15**, **9** and **10**. Reaction time 12 h, colorless microcrystals from ethanol, m.p. 164-166 °C, yield (1.45 g) 56%. IR ν (cm^{-1}): 1713, 1605, 1463. ^{1}H-NMR (500 MHz, $CDCl_3$) δ (ppm): 2.16 (s, 3H), 2.24 (s, 3H), 2.27 (s, 3H), 2.39 (br s, 4H), 2.50 (br s, 4H), 2.71 (d, J = 17.6 Hz, 1H), 3.02 (d, J = 17.6 Hz, 1H), 3.58 (t, J = 8.8 Hz, 1H), 4.06 (t, J = 9.6 Hz, 1H), 4.24 (d, J = 13.0 Hz, 1H), 4.34-4.40 (m, 2H), 6.70-7.65 (m, 12H). ^{13}C-NMR (125 MHz, $CDCl_3$) δ (ppm): 21.2, 35.3, 35.5, 46.1, 49.6, 50.6, 54.9, 59.1, 61.9, 66.9, 78.2, 109.4, 122.8, 124.0, 125.2, 125.5, 127.3, 129.2, 130.0, 134.5, 135.9, 136.1, 136.7, 143.8, 151.8, 177.2, 206.7. HRMS (+ESI-TOF) *m/z* for $C_{33}H_{36}N_4O_2$ $[M + 1]^+$ calcd 521.2917, found 521.2935.

4'-(4-Methoxyphenyl)-1'-methyl-1''-[(1-piperidinyl)methylene]-dispiro[2*H*-indene-2,3'-pyrrolidine-2',3''-[3*H*]indole]-1,2''(1''*H*, 3*H*)-dione (30)

Obtained from reaction of **16**, **7** and **10**. Reaction time 1.5 h, colorless microcrystals from ethanol, m.p. 126-128 °C, yield (1.55 g) 60%. IR ν (cm^{-1}): 1717, 1603, 1511. ^{1}H-NMR (500 MHz, $CDCl_3$) δ (ppm): 1.35-1.48 (m, 6H), 2.15 (s, 3H), 2.39 (br d, 4H), 2.72 (d, J = 17.6 Hz, 1H), 3.07 (d, J = 17.6 Hz, 1H), 3.57 (t, J = 8.8 Hz, 1H), 3.72 (s, 3H), 4.02 (t, J = 9.6 Hz, 1H), 4.18 (d, J = 13.0 Hz, 1H), 4.35-4.44 (m, 2H), 6.75-7.46 (m, 12H). ^{13}C-NMR (125 MHz, $CDCl_3$) δ (ppm): 24.0, 25.8, 35.2, 35.4, 49.3, 52.1, 55.3, 59.2, 62.7, 66.8, 78.2, 109.4, 113.9, 122.7, 124.0, 124.2, 125.2, 125.5, 127.3, 129.1, 131.1, 134.5, 136.0, 144.3, 151.8, 158.6, 177.4, 206.8. Elemental analysis: $C_{33}H_{35}N_3O_3$ required C, 75.98; H, 6.76; N, 8.05, found C, 75.61; H, 6.85; N, 7.72.

4'-(4-Methoxyphenyl)-1'-methyl-1''-[(4-morpholinyl)methylene]-dispiro[2*H*-indene-2,3'-pyrrolidine-2',3''-[3*H*]indole]-1,2''(1''*H*, 3*H*)-dione (31)

Obtained from reaction of **16**, **8** and **10**. Reaction time 10 h, colorless microcrystals from *n*-butanol, m.p. 188-190 °C, yield (1.45 g) 55%. IR ν (cm^{-1}): 1723, 1708, 1607, 1516. ^{1}H-NMR (500 MHz, $CDCl_3$) δ (ppm): 2.16 (s, 3H), 2.38-2.48 (m, 4H), 2.73 (d, J = 17.6 Hz, 1H), 3.07 (d, J = 17.6 Hz, 1H), 3.56-3.65 (m, 5H), 3.75 (s, 3H), 4.02 (t, J = 9.2 Hz, 1H), 4.22 (d, J = 13.0 Hz, 1H), 4.37-4.42 (m, 2H), 6.73-7.47 (m, 12H). ^{13}C-NMR (125 MHz, $CDCl_3$) δ (ppm): 35.1, 35.5, 49.2, 51.0, 55.3, 59.1, 62.1, 66.8, 66.9, 78.3, 109.2, 113.9, 122.9, 124.0, 125.2, 125.5, 127.3, 127.5, 129.2, 131.1, 134.6, 135.9, 143.8, 151.8, 158.6, 177.4, 206.5. Elemental analysis: $C_{32}H_{33}N_3O_4$ required C, 73.40; H, 6.35; N 8.02, found C, 73.71; H, 6.61; N, 7.75.

1'-Methyl-1''-[(1-piperidinyl)methylene]-4'-(3,4,5-trimethoxyphenyl)-dispiro[2*H*-indene-2,3'-pyrrolidine-2',3''-[3*H*]indole]-1,2''(1''*H*, 3*H*)-dione (32)

Obtained from reaction of **17**, **7** and **10**. Reaction time 1.5 h, colorless microcrystals from ethanol, m.p. 116-117 °C, yield (1.65 g) 57%. IR ν (cm^{-1}): 1713, 1606, 1589. ^{1}H-NMR (500 MHz, $CDCl_3$) δ (ppm): 1.37-1.50 (m, 6H), 2.16 (s, 3H), 2.42 (br d, 4H), 2.68 (d, J = 17.6 Hz, 1H), 3.04 (d, J = 17.6 Hz, 1H), 3.62 (t, J = 8.8 Hz, 1H), 3.76 (s, 6H), 3.79 (s, 3H), 4.05 (t, J = 9.2 Hz, 1H), 4.14 (d, J = 12.2 Hz, 1H), 4.30 (t, J = 8.8 Hz, 1H), 4.50 (d, J = 13.0 Hz, 1H), 6.67-7.49 (m, 10H). ^{13}C-NMR (125 MHz, $CDCl_3$) δ (ppm): 24.1, 25.9, 35.4, 50.3, 52.1, 56.1, 59.2, 60.9, 62.7, 66.9, 78.1, 106.8, 109.4, 122.7, 124.0, 124.2, 125.0, 125.5, 127.2, 127.3, 129.2, 134.6, 135.1, 136.0, 136.7, 144.4, 151.9, 153.0, 177.5, 206.8. Elemental analysis: $C_{35}H_{39}N_3O_5$ required C, 72.27; H, 6.76; N, 7.22, found C, 71.96; H, 6.73; N, 6.95.

1'-Methyl-1''-[(4-morpholinyl)methylene]-4'-(3,4,5-trimethoxyphenyl)-dispiro[2*H*-indene-2,3'-pyrrolidine-2',3''-[3*H*]indole]-1,2''(1''*H*, 3*H*)-dione (33)

Obtained from reaction of **17**, **8** and **10**. Reaction time 2.5 h, colorless microcrystals from ethanol, m.p. 113-115 °C, yield (1.75 g) 60%. IR ν (cm^{-1}): 1712, 1593, 1505. ^{1}H-NMR (500 MHz, $CDCl_3$) δ (ppm): 2.16 (s, 3H), 2.44 (m, 4H), 2.69 (d, J = 17.6 Hz, 1H), 3.04 (d, J = 17.6 Hz, 1H), 3.62 (br s, 4H) 3.72-3.82 (m, 10H), 4.04 (t, J = 9.2 Hz, 1H), 4.19 (d, J = 13.0 Hz, 1H), 4.32 (t, J = 8.8 Hz, 1H), 4.45 (d, J = 13.5 Hz, 1H), 6.58-7.54 (m, 10H). ^{13}C-NMR (125 MHz, $CDCl_3$) δ (ppm): 35.3, 35.4, 50.2, 51.0, 56.1, 59.0, 60.9, 62.1, 66.8, 66.9, 78.2, 106.8, 109.2, 122.9, 124.1, 125.0, 125.6, 127.4, 128.0, 129.3, 134.9, 135.9, 136.7, 143.9, 151.9, 153.1, 177.4, 206.6. Elemental analysis: $C_{34}H_{37}N_3O_6$ required C, 69.97; H, 6.39; N, 7.20, found C, 70.06; H, 6.43; N, 7.36.

4'-(4-Dimethylaminophenyl)-1'-methyl-1''-[(1-piperidinyl)methylene]-dispiro[2*H*-indene-2,3'-pyrrolidine-2',3''-[3*H*]indole]-1,2''(1''*H*, 3*H*)-dione (34)

Obtained from reaction of **18**, **7** and **10**. Reaction time 1.5 h, yellow microcrystals from ethanol, m.p. 125-127 °C, yield (1.20 g) 45%. IR ν (m^{-1}): 1708, 1605, 1522. ^{1}H-NMR (300 MHz, $CDCl_3$) δ (ppm): 1.37-1.54 (m, 6H), 2.18 (s, 3H), 2.33-2.48 (m, 4H), 2.82 (d, J = 18.0 Hz, 1H), 2.91 (s, 6H), 3.15 (d, J = 17.7 Hz, 1H), 3.57 (t, J = 8.6 Hz, 1H), 4.05 (t, J = 9.5 Hz, 1H), 4.18 (d, J = 12.9 Hz, 1H), 4.40 (t, J = 8.6 Hz, 1H), 4.45 (d, J = 12.6 Hz, 1H), 6.63-7.64 (m, 12H). Elemental analysis: $C_{34}H_{38}N_4O_2$ required C, 76.37; H, 7.16; N, 10.48, found C, 76.51; H, 7.22; N, 10.59.

4'-(4-Dimethylaminophenyl)-1'-methyl-1''-[(4-morpholinyl)methylene]-dispiro[2*H*-indene-2,3'-pyrrolidine-2',3''-[3*H*]indole]-1,2''(1''*H*, 3*H*)-dione (35)

Obtained from reaction of **18**, **8** and **10**. Reaction time 1.5 h, yellow microcrystals from ethanol, m.p. 156-158 °C, yield (1.55 g) 58%. IR ν (cm^{-1}): 1702, 1605, 1523. ^{1}H-NMR (300 MHz, $CDCl_3$) δ (ppm): 2.18 (s, 3H), 2.37-2.51 (m, 4H), 2.83 (d, J = 17.7 Hz, 1H), 2.90 (s, 6H), 3.15 (d, J = 17.4 Hz, 1H), 3.57 (t, J = 9.0 Hz, 1H), 3.62 (t, J = 4.7 Hz, 4H), 4.04 (t, J = 9.3 Hz, 1H), 4.20 (d, J = 12.6 Hz, 1H), 4.41 (t, J = 9.6 Hz, 1H), 4.42 (d, J = 12.6 Hz, 1H), 6.63-7.48 (m, 12H). Elemental analysis: $C_{33}H_{36}N_4O_3$ required C, 73.86; H, 6.76; N, 10.44, found C, 74.15; H, 6.67; N, 10.18.

1'-methyl-1''-[(1-piperidinyl)methylene]-4'-(2-thienyl)-dispiro[2*H*-indene-2,3'-pyrrolidine-2',3''-[3*H*]indole]-1,2''(1''*H*, 3*H*)-dione (36)

Obtained from reaction of **19**, **7** and **10**. Reaction time 12 h, colorless microcrystals from *n*-butanol, m.p. 184-185 °C, yield (1.10 g) 44%. IR ν (cm^{-1}): 1706, 1604, 1464. ^{1}H-NMR (500 MHz, $CDCl_3$) δ (ppm): 1.34-1.55 (m, 6H), 2.17 (s, 3H), 2.39 (br d, 4H), 2.84 (d, J = 17.8 Hz, 1H), 3.14 (d, J = 17.8 Hz, 1H), 3.70 (t, J = 9.4 Hz, 1H), 4.07 (t, J = 9.5 Hz, 1H), 4.21 (d, J = 13.2 Hz, 1H), 4.44 (d, J = 12.6 Hz, 1H), 4.69 (t, J = 9.2 Hz, 1H), 6.81-7.56 (m, 11H). ^{13}C-NMR (125 MHz, $CDCl_3$) δ (ppm): 24.0, 25.8, 34.5, 35.5, 44.9, 52.0, 59.7, 62.7, 66.4, 78.0, 109.6, 122.7, 124.1, 124.8, 125.6, 127.0, 127.4, 129.3, 134.8, 136.0, 142.5, 152.3, 177.1, 206.1. Elemental analysis: $C_{30}H_{31}N_3O_2S$ required C, 72.41; H, 6.28; N, 8.44, found C, 72.49; H, 6.40; N, 8.13.

4'-(2,4-Dichlorophenyl)-1'-methyl-dispiro[2*H*-indene-2,3'-pyrrolidine-2',3''-[3*H*]indole]-1,2''(1''*H*, 3*H*)-dione (37)

Obtained from reaction of **14**, **9** and **10**. Reaction time 2 h, colorless microcrystals from *N,N*-dimethylformamide, m.p. 255-257 °C, yield (1.20 g) 52%. IR ν (cm^{-1}): 1717, 1611, 1469. ^{1}H-NMR (500 MHz, DMSO-d_6) δ (ppm): 2.01 (s, 3H), 2.38 (d, J = 18.4 Hz, 1H), 2.79 (d, J = 18.4 Hz, 1H,), 3.44 (t, J = 8.0 Hz, 1H), 3.91 (t, J = 8.8 Hz, 1H), 4.59 (t, J = 8.4 Hz, 1H), 6.50-8.07 (m, 11H), 10.60 (s, 1H). Elemental analysis: $C_{26}H_{20}Cl_2N_2O_2$ required C, 67.40; H, 4.35; N, 6.05, found C, 67.48; H, 4.22; N, 5.94.

4'-(2,4-Dimethylaminophenyl)-1'-methyl-dispiro[2*H*-indene-2,3'-pyrrolidine-2',3''-[3*H*]indole]-1,2''(1''*H*, 3*H*)-dione (38)

Obtained from reaction of **18**, **9** and **10**. Reaction time 1.5 h, yellow microcrystals from *n*-butanol, m.p. 239-240 °C, yield (1.30 g) 59%. IR ν (cm^{-1}): 1709, 1614, 1523. ^{1}H-NMR (500 MHz, DMSO-d_6) δ (ppm): 2.08 (s, 3H), 2.64 (d, J = 17.6 Hz, 1H), 2.81 (s, 6H), 3.09 (d, J = 16.8 Hz, 1H), 3.46 (br s, 1H), 3.88 (t, J = 8.8 Hz, 1H), 4.15 (t, J = 8.8 Hz, 1H), 6.58-7.40 (m, 12H), 10.52 (s, 1H). ^{13}C-NMR (125 MHz, DMSO-d_6) δ (ppm): 34.8, 35.2, 49.6, 58.9, 66.3, 78.0, 109.8, 112.8, 121.9, 123.6, 126.3, 126.7, 127.4, 127.9, 129.5, 130.7, 135.3, 135.8, 143.0, 149.8, 152.2, 178.1, 206.7. Elemental analysis: $C_{28}H_{27}N_3O_2$ required C, 76.86; H, 6.22; N, 9.60, found C, 76.59; H, 6.45; N, 9.30.

Antitumor activity screening

Establishment of primary cultures from tumors isolated from patients with metastatic melanoma

Tumor specimens (at least 1 g) were placed in Petri dishes containing RPMI 1640 + 10% FCS. After eliminating non-tumor and necrotic parts, tissue was dissected into small pieces with a scalpel, squeezing each piece to produce cell suspensions. Cell suspension was filtered through sterile gauze to eliminate macroscopic debris. Cell suspension was checked for cellular composition. In the presence of significant red blood cell

contamination, treatment with ACK (10 minutes in ice) was performed, the samples were centrifuged and dead cells eliminated by digestion with DNase and trypsin. Viability of cell suspension is checked by trypan blue exclusion. In cases where the number of tumor cells obtained from the mechanical processing was not adequate, the remaining tumor tissue fragments were treated with a series of enzymes: DNase (200 μl/ml), Collagenase (0.1%), Hyaluronidase (2.5 μl/ml), Trypsin (0.5 mg/ml)**.** Following 45 minute incubation at room temperature on a magnetic shaker, cell suspension was filtered through sterile gauze to remove debris. Cell suspension was recovered from the supernatant by centrifugation and extensively washed in RPMI 1640 + 10% FCS. Part of the cell suspension was then place in a culture in complete medium, while a part was frozen in aliquots. Cells were periodically characterized by immunohystochemistry staining with S100, MelanA and HMB45 antibodies at various passages during the time they are kept in culture.

Cell culture

GaLa, LuPiCi, and LuCa cells were isolated from patients with LN metastatic melanoma according to the protocol described above. Cells were grown in DMEM medium supplemented with 5% fetal bovine serum, 2 mM glutamine. All cultures were maintained in a humidified tissue culture incubator at 37 °C in 5% CO_2.

***In-vitro* Viability Assay**

The anticancer potential of the tested compounds was explored against GaLa, LuPiCi and LuCa cells (human metastatic melanoma): cells were plated at 5000 cells/well in 96 well plate and treated 24 h later with varying concentrations of the tested compounds, doxorubicin was used as a positive control, for 48 h obeying the standard reported procedure.[23-31] Cells were seeded in 96-well microtiter plates in a fresh medium and left for 24 h before treatment with the tested compounds to allow attachment of cells to the wall of the plate. The tested compounds were dissolved in dimethylsulfoxide (DMSO) and diluted 1000-fold in the assay. Different concentrations of the compounds under test were added to the cell monolayer. Triplicate wells were prepared for each individual dose. The monolayer cells were incubated with the tested compounds for 48 h at 37 °C, in atmosphere of 5% CO_2. After 48 h, the cells were fixed, washed and stained with Sulfo-Rhodamine-B (SRB) stain. Excess stain was washed with acetic acid. The attached stain was recovered with Tris-EDTA buffer. Cell viability was determined by the CellTiter-Glo® Luminescent Cell Viability Assay (Promega). Data were collected as mean values for experiments that were performed in three replicates for each individual dose and measured. The cell surviving fraction was calculated by equation (5).

Surviving fraction = Optical density (O.D.) of treated cells/O.D. of control cells…..... (5)

The IC_{50} (concentration required to produce 50% inhibition of cell growth compared to the control experiment) was determined using Graph-Pad PRISM version-5 software. Statistical calculations for determination of the mean and standard error values were detected by SPSS software. The observed antitumor properties are presented in Table 1.

Acknowledgements

This study was supported financially by the Science and Technology Development Fund (STDF), Egypt, Grant No. 1357.

Notes and references

[a]Pesticide Chemistry Department, National Research Centre, Dokki, Giza 12622, Egypt.
[b]Center for Heterocyclic Compounds, Department of Chemistry, University of Florida, Gainesville, FL 32611-7200, USA.
[c]Therapeutical Chemistry Department, National Research Centre, Dokki, Giza 12622, Egypt.
[d]Pharmaceutical Chemistry Department, Faculty of Pharmacy, Ain Shams University, Cairo, Egypt.
[e]Department of Experimental Oncology at the IFOM-IEO Campus, European Institute of Oncology, IEO, 20139 Milan, Italy.
[f]Pharmacology and Toxicology Department, Faculty of Pharmacy, Ain Shams University, Cairo, Egypt.
*Corresponding authors: Adel S. Girgis, Fax: +33370931; Tel: +01220447199, e-mail: girgisas10@yahoo.com

† Electronic Supplementary Information (ESI) available: [including Tables of two descriptor models of the GaLa, LuPiCi and LuCa carcinoma cell lines, molecular descriptor values and QSAR model due to mean IC_{50} values of the three carcinoma cell lines, in addition to the figures of the GaLa, LuPiCi and LuCa carcinoma cell lines 3D-pharmacophore mapped on the synthesized spiro-alkaloids and 2D-QSAR models]. See DOI: 10.1039/b000000x/

‡ Professor Alan R. Katritzky passed away10th February 2014.

1 H. Guo and Y. Miao, *Bioorg. Med. Chem. Letters*, 2013, **23**, 2319–2323.
2 H. J. Kim, H. J. Cho, H. Kim, M. I. El-Gamal, C.-H. Oh, S. H. Lee, T. Sim, J.-M. Hah and K. H. Yoo, *Bioorg. Med. Chem. Letters*, 2012, **22**, 3269–3273.
3 C. Garbe, A. Hauschild, M. Volkenandt, D. Schadendorf, W. Stolz, U. Reinhold, R. D. Kortmann, C. Kettelhack, B. Frerich, U. Keilholz, R. Dummer, G. Sebastian, W. Tilgen, G. Schuler, A. Mackensen and R. Kaufmann, *Melanoma Res.*, 2007, **17**, 393–399.
4 S. J. Divito and L. K. Ferris, *Melanoma Res.*, 2010, **20**, 450–458.
5 C. M. Balch, A. C. Buzaid, S. J. Soong, M. B. Atkins, N. Cascinelli, D. G. Coit, I. D. Fleming, J. E. Gershenwald, A. Jr. Houghton, J. M. Kirkwood, K. M. McMasters, M. F. Mihm, D. L. Morton, D. S. Reintgen, M. I. Ross, A. Sober, J. A. Thompson and J. F. Thompson, *J. Clin. Oncol.*, 2001, **19**, 3635–36348.
6 M. L. Lee, K. Tomsu and K. B. Von Eschen, *Melanoma Res.*, 2000, **10**, 81–92.

7 M.-H. Jung, M. I. El-Gamal, M. S. Abdel-Maksoud, T. Sim, K. H. Yoo and C.-H. Oh, *Bioorg. Med. Chem. Letters*, 2012, **22**, 4362–4367.
8 L. Zhang, Q. Zheng, Y. Yang, H. Zhou, X. Gong, S. Zhao and C. Fan, *Eur. J. Med. Chem.*, 2014, **82**, 139−151.
9 S. Faivre, G. Demetri, W. Sargent and E. Raymond, *Nat. Rev. Drug Discov.*, 2007, **6**, 734−745.
10 T. J. Abrams, L. B. Lee, L. J. Murray, N. K. Pryer and J. M. Cherrington, *Mol. Cancer Ther.*, 2003, **2**, 471−478.
11 D. B. Mendel, A. D. Laird, X. Xin, S. G. Louie, J. G. Christensen, G. Li, R. E. Schreck, T. J. Abrams, T. J. Ngai, L. B. Lee, L. J. Murray, J. Carver, E. Chan, K. G. Moss, J. O. Haznedar, J. Sukbuntherng, R. A. Blake, L. Sun, C. Tang, T. Miller, S. Shirazian, G. McMahon and J. M. Cherrington, *Clin. Cancer Res.*, 2003, **9**, 327−337.
12 H. Prenen, J. Cools, N. Mentens, C. Folens, R. Sciot, P. Schoffski, A. Van Oosterom, P. Marynen and M. Debiec-Rychter, *Clin. Cancer Res.* 2006, **12**, 2622−2627.
13 E. Garcia Prado, M. D. Garcia Gimenez, R. De la PuertaVázquez, J. L. Espartero Sánchez and M. T. Sáenz Rodriguez, *Phytomedicine*, 2007, **14**, 280−284.
14 C. B. Cui, H. Kakeya and H. Osada, *Tetrahedron*, 1996, **52**, 12651−12666.
15 C. B. Cui, H. Kakeya and H. Osada, *J. Antibiot.*, 1996, **49**, 832−835.
16 Y. Zhao, S. Yu, W. Sun, L. Liu, J. Lu, D. McEachern, S. Shargary, D. Bernard, X. Li, T. Zhao, P. Zou, D. Sun and S. Wang, *J. Med. Chem.*, 2013, **56**, 5553−5561.
17 C. Mondal, A. K. Halder, N. Adhikari, A. Saha, K. D. Saha, S. Gayen and T. Jha, *Eur. J. Med. Chem.*, 2015, **90**, 860−875.
18 Q. Ding, Z. Zhang, J. Liu, N. Jiang, J. Zhang, T. M. Ross, X. J. Chu, D. Bartkovitz, F. Podlaski, C. Janson and B. Graves, *J. Med. Chem.*, 2013, **56**, 5979−5983.
19 Y. Rew and D. Sun, *J. Med. Chem.*, 2014, **57**, 6332−6341.
20 Y. Zhao, S. Yu, W. Sun, L. Liu, J. Lu, D. McEachern, S. Shargary, D. Bernard, X. Li, T. Zhao, P. Zou, D. Sun and S. Wang, *J. Med. Chem.*,2013, **56**, 5553−5561.
21 A. Kumar, G. Gupta, A. K. Bishnoi, R. Saxena, K. S. Saini, R. Konwar, S. Kumar and A. Dwivedi, *Bioorg. Med. Chem.*, 2015, **23**, 839–848.
22 R. Grigg and S. Thianpatanagul, *J. Chem. Soc., Chem. Commun.*, 1984, 180–181.
23 A. M. Moustafa, A. S. Girgis, S. M. Shalaby and E. R. T. Tiekink, *Acta Crystallogr.,* 2012, **E68**, o2197–o2198.
24 A. S. Girgis, *Eur. J. Med. Chem.*, 2009, **44**, 91–100.
25 A. S. Girgis, S. S. Panda, E. M. Shalaby, A. F. Mabied, P. J. Steel, C. D. Hall and A. R. Katritzky, *RSC Advances*, 2015, **5**, 14780−14787.
26 A. S. Girgis, S. S. Panda, I. S. Ahmed Farag, A. M. El-Shabiny, A. M. Moustafa, N. S. M. Ismail, G. G. Pillai, C. S. Panda, C. D. Hall and A. R. Katritzky, *Org. Biomol. Chem.*, 2015, **13**, 1741−1753.
27 R. F. George, N. S. M. Ismail, J. Stawinski and A. S. Girgis, *Eur. J. Med. Chem.* 2013, **68**, 339−351.
28 A. S. Girgis, J. Stawinski, N. S. M. Ismail and H. Farag, *Eur. J. Med. Chem.* 2012, **47**, 312−322.
29 A. R. Katritzky, A. S. Girgis, S. Slavov, S. R. Tala and I. Stoyanova-Slavova, *Eur. J. Med. Chem.*, 2010, **45**, 5183−5199.
30 A. S. Girgis, *Eur. J. Med. Chem.*, 2009, **44**, 1257–1264.
31 A. S. Girgis, H. M. Hosni and F. F. Barsoum, *Bioorg. Med. Chem.*, 2006, **14**, 4466−4476.
32 C. G. Wermuth, C. R. Ganellin, P. Lindberg and L. A. Mitscher, *Annu. Rep. Med. Chem.*, 1998, **33**, 385−395.
33 A. S. Girgis, H. Farag, N. S. M. Ismail and R. F. George, *Eur. J. Med. Chem.*, 2011, **46**, 4964−4969.
34 A. S. Girgis, N. S. M. Ismail and H. Farag, *Eur. J. Med. Chem.*, 2011, **46**, 2397−2407.
35 A. S. Girgis, N. S. M. Ismail, H. Farag, W. I. El-Eraky, D. O. Saleh, S. R. Tala and A. R. Katritzky, *Eur. J. Med. Chem.*, 2010, **45**, 4229−4238.
36 A. D. Tiwari, S. S. Panda, A. S. Girgis, S. Sahu, R. F. George, A. M. Srour, B. La Starza, A. M. Asiri, C. D. Hall and A. R. Katritzky, *Org. Biomol. Chem.*, 2014, **12**, 7238−7249.
37 E. M. Shalaby, A. S. Girgis, A. M. Moustafa, A. M. ElShaabiny, B. E. M. El-Gendy, A. F. Mabied and I. S. Ahmed Farag, *J. Mol. Structure*, 2014, **1075**, 327−334.
38 A. S. Girgis, S. S. Panda, E. M. Shalaby, A. F. Mabied, P. J. Steel, C. D. Hall and A. R. Katritzky, *RSC Advances*, 2015, **5**, 14780−14787.
39 A. S. Girgis, S. S. Panda, M. N. Aziz, P. J. Steel, C. D. Hall and A. R. Katritzky, *RSC Advances*, 2015, **5**, 28554–28569.
40 A.B. Sannigrahi, *Adv. Quant. Chem.,* 1992, **23**, 301–351.
41 CODESSA-Pro manual pp 54, 59, 68.
42 V. R. Solomon, C. Hu and H. Lee, *Bioorg. Med. Chem.*, 2009, **17**, 7585–7592.
43 A. T. Taher, N. A. Khalil and E. M. Ahmed, *Arch Pharm. Res.*, 2011, **34**, 1615–1621.
44 N. El-Rayyes, S. AI-Qatami and M. Edun, *J. Chem. Engineering Data*, 1987, **32**, 481–483.
45 Y. Poirier and N. Lozac'h, *Bull. Soc. Chim. France*, 1966, 1052–1068.
46 F. Fournier, J. Berthelot, A.-M. Pavard, N. Ronzani and J.-J. Basselier, *Eur. J. Med. Chem.*, 1981, **16**, 48–58.
47 G. Narang, D. P. Jindal, B. Jit, R. Bansal, B. S. Potter and R. A. Palmer, *Helv. Chim. Acta*, 2006, **89**, 258–264.
48 R. Bansal, G. Narang, C. Zimmer and R. W. Hartmann, *Med. Chem. Res.*, 2011, **20**, 661–669.